

**RESEARCH ARTICLE**

10.1029/2022MS003578

**Key Points:**

- The global simulation of the Madden–Julian oscillation (MJO) with a new spectral convection scheme named stochastic unified convection scheme (UNICON) is evaluated
- Stochastic UNICON improves various properties of the simulated MJO compared to the non-stochastic version
- The increased shallow convection in stochastic UNICON leads to a stronger moistening tendency in MJO developing stage

**Supporting Information:**

Supporting Information may be found in the online version of this article.

**Correspondence to:**

J.-J. Baik,  
jjbaik@snu.ac.kr

**Citation:**

Shin, J., & Baik, J.-J. (2023). Global simulation of the Madden–Julian oscillation with stochastic unified convection scheme. *Journal of Advances in Modeling Earth Systems*, 15, e2022MS003578. <https://doi.org/10.1029/2022MS003578>

Received 12 DEC 2022

Accepted 23 JUN 2023

© 2023 The Authors. Journal of Advances in Modeling Earth Systems published by Wiley Periodicals LLC on behalf of American Geophysical Union. This is an open access article under the terms of the Creative Commons Attribution-NonCommercial-NoDerivs License, which permits use and distribution in any medium, provided the original work is properly cited, the use is non-commercial and no modifications or adaptations are made.

## Global Simulation of the Madden–Julian Oscillation With Stochastic Unified Convection Scheme

Jihoon Shin<sup>1</sup>  and Jong-Jin Baik<sup>1</sup> <sup>1</sup>School of Earth and Environmental Sciences, Seoul National University, Seoul, South Korea

**Abstract** A new spectral convection scheme, the stochastic unified convection scheme (stochastic UNICON), is implemented in a general circulation model. The global climate simulation using stochastic UNICON is evaluated and compared with UNICON, focusing on the simulation of the Madden–Julian oscillation (MJO). Stochastic UNICON extends the original UNICON by randomly sampling convective updrafts from the joint probability density function constructed at the near-surface, generating a spectrum of convective updrafts in a physically based manner. The performances of UNICON and stochastic UNICON on simulating observed mean climates are comparable, while stochastic UNICON slightly reduces the mean bias of climate variables. For the simulation of intraseasonal variabilities, stochastic UNICON outperforms UNICON in many aspects. Stochastic UNICON improves the simulation of the intensity and propagation patterns of boreal winter MJO, which are too weakly simulated in UNICON. The coherency between MJO-related convection and large-scale circulation is also enhanced, which many climate models underestimate. The improvement of MJO simulation by stochastic UNICON is related to a better representation of the relationship between moisture and convection in the model. The increased frequency of shallow convection in stochastic UNICON leads to stronger moisture convergence that precedes convection activity peak and results in the more robust development of organized convection and more frequent intense precipitation. A precipitation budget analysis reveals that the moisture tendencies due to horizontal advection and convective process are consistently enhanced during MJO developing periods by stochastic UNICON.

**Plain Language Summary** The Madden–Julian oscillation (MJO) emerges in the tropics as a pattern of rainy periods followed by dry periods that fluctuates on weekly to monthly time scales. The MJO is important for various weather and climate phenomena but poorly represented in global climate models (GCMs). To simulate realistic MJO, convection needs to be realistically modeled. Recently, a new spectral convection scheme named stochastic unified convection scheme (stochastic UNICON) is developed based on the unified convection scheme (UNICON). Stochastic UNICON can represent different types of convective clouds in a model grid. The GCM with stochastic UNICON simulates better strength and propagation of winter MJO and better relationship between convection and large-scale circulation compared to that of UNICON. The improvements come from a more realistic relationship between moisture and convection. The increased frequency of shallow convection in stochastic UNICON produces the condition for the MJO to develop more robustly.

### 1. Introduction

The Madden–Julian oscillation (MJO; Madden & Julian, 1971) is the dominant mode of intraseasonal variability in the tropical atmosphere. It is characterized by eastward-propagating envelopes of convective cloud clusters that are coupled with large-scale atmospheric circulation. The MJO interacts with a variety of weather and climate phenomena, including monsoonal system (Lavender & Matthews, 2009; Lorenz & Hartmann, 2006; Singh et al., 1992; Taraphdar et al., 2018), El Niño–Southern Oscillation (Hendon et al., 2007; Lee et al., 2019; Moon et al., 2011), and tropical cyclone activity (Camargo et al., 2009; Hall et al., 2001; Liebmann et al., 1994; Maloney & Hartmann, 2000a, 2000b). The ability of global climate models (GCMs) to accurately simulate the intensity, spatial structure, and dispersion relation of the MJO is critical for predicting tropical variabilities and their future projections.

Despite the importance, state-of-art GCMs still have shortcomings in realistically simulating the MJO. Most models participating in Coupled Model Intercomparison Project Phase 5 (CMIP5) simulate underestimated MJO amplitude and low coherency between large-scale wind field and convection system (Ahn et al., 2017). With

considerable improvement in physics parameterizations, the general performance on the simulation of the MJO is improved in the CMIP6 models compared to the CMIP5 models (Ahn et al., 2020; G. Chen et al., 2022; Orbe et al., 2020). However, many CMIP6 models still underestimate MJO amplitude and struggle to simulate realistic eastward propagation patterns (G. Chen et al., 2022; Le et al., 2021). The realistic representation of the MJO in GCMs is a challenging task in that it involves physical processes with large uncertainties. Particularly, parameterizing subgrid-scale convection is thought to account for a large portion of the uncertainties because of the stochastic nature of atmospheric convection. One important issue related to MJO simulation is the parameterization of organized convection. The MJO is associated with squall lines and mesoscale convective systems, which have substantially different characteristics from unorganized convection (e.g., S. S. Chen et al., 1996; Powell & Houze, 2013). C.-C. Chen et al. (2021) implemented an organized convection parameterization in a GCM and reported that the organized convection parameterization improves the representation of the MJO and reduces precipitation biases over the tropics.

Another important component in convection parameterizations that can significantly affect the performance of MJO simulations is the spectral and/or stochastic representation of convective clouds. In a typical grid size of a GCM, a spectrum of convective clouds is formed in a stochastic way. It is important to represent the coexistence of shallow and deep convection since shallow convection supplies moisture to the lower troposphere to sustain organized convection in developing MJO (Benedict & Randall, 2007; Cai et al., 2013; Janiga & Zhang, 2016; G. J. Zhang & Song, 2009). In addition, cloud systems in developing MJO undergo a transition from shallow to deep convection, so there is an emerging demand for developing convection parameterization that represents different types of convection in a continuous and unified way. Several spectral convection schemes have been proposed to represent different cloud types (Baba, 2019; Neggers, 2015; Suselj et al., 2019; B. Yang et al., 2021; Yoshimura et al., 2015). The spectral convection schemes typically set the distribution of a quantity that is thought to control the variability of convective clouds; These quantities are, for example, cloud base updraft velocity (Baba, 2019), cloud size (Neggers, 2015), and entrainment rate (B. Yang et al., 2021; Yoshimura et al., 2015). Global simulations with these schemes have shown improvements in the intensity and frequency of the simulated MJO without degrading mean climatology (Baba, 2021; Baba & Giorgetta, 2020). The results from the aforementioned GCM experiments suggest that spectral convection parameterization and organized convection parameterization can alleviate a problem known as “MJO-mean state trade-off” in GCMs, a problem where modifications in the convection parameterizations that improve MJO simulation tend to degrade the mean state (Ahn et al., 2019; B. Chen & Mapes, 2018; Hannah & Maloney, 2011; Kim et al., 2011).

Unified convection scheme (UNICON; Park, 2014) is one of the rare schemes which simulate subgrid mesoscale organized flow and its impacts on subgrid convection in an explicit way. UNICON was implemented into a GCM and participated in CMIP6 under the name of Seoul National University Atmosphere Model Version 0 with a UNICON (SAM0-UNICON; Park et al., 2019). SAM0-UNICON is based on the Community Atmosphere Model Version 5 (CAM5; Park et al., 2014), but CAM5's shallow and deep convection schemes were replaced by UNICON. SAM0-UNICON simulates relatively good intraseasonal variability compared to other CMIP6 models, showing the second rank among 20 models in the model evaluation using wavelet-based spectral principal component analysis (Le et al., 2021). SAM0-UNICON also realistically reproduces the observed impact of MJO on tropical cyclone activity (Shin & Park, 2020a).

Shin and Park (2020b) (SP20 hereinafter) developed a stochastic unified convection scheme (stochastic UNICON) for shallow convection based on UNICON, and Shin and Baik (2023) (SB23 hereinafter) extended it for deep convection. Stochastic UNICON extends UNICON, a bulk plume model, to a spectral (and stochastic) plume model that computes the mean and variance of physical tendencies generated by an ensemble of convective updrafts and downdrafts. Stochastic UNICON generates a spectrum of convective updrafts by constructing a joint probability density function (PDF) of convective updraft properties at the near-surface and initializing convective updrafts randomly from the joint PDF. Stochastic UNICON differs from other spectral schemes in that the joint PDF is constructed for all fundamental properties of convective updrafts (thermodynamic variables, horizontal and vertical velocities, and updraft radius) in a physically based manner. The evaluation with a single-column model (SCM) showed that stochastic UNICON reduces biases presented in original UNICON for tropical convection cases (SB23).

In this study, we evaluate the global simulation of stochastic UNICON, focusing on the intraseasonal variability represented by the MJO. Two climate simulations of SAM0-UNICON atmospheric GCM with UNICON and

stochastic UNICON are compared and evaluated against observations. First, we demonstrate the model diagnostics on the simulations of global climatologies and discuss spatial distributions of the model biases. Next, various model diagnostics for the MJO are presented to demonstrate the impacts of the spectral parameterization. To understand the physical processes of simulated MJO, we conduct the precipitation budget analysis of Adames (2017). We deeply discuss the simulated relationship between moisture and precipitation and how the spectral representation of convection helps improve the moisture–precipitation relationship and MJO simulation.

## 2. Methods

### 2.1. Stochastic UNICON

Stochastic UNICON constructs a joint PDF of updraft radius  $R$  and updraft thermodynamic properties  $\phi = w, \theta_c, q_p, u, v, \xi$ , where  $w$  is the vertical velocity;  $\theta_c \equiv \theta - (L_v/c_p)\pi q_l - (L_s/c_p)\pi q_i$  is the condensate potential temperature, where  $\theta$  is the potential temperature,  $L_v$  and  $L_s$  are the latent heats of vaporization and sublimation, respectively,  $c_p$  is the specific heat at constant pressure, and  $\pi$  is the Exner function;  $q_t \equiv q_v + q_l + q_i$  is the total water specific humidity, where  $q_v, q_l$ , and  $q_i$  are the specific humidities of water vapor, liquid, and ice, respectively;  $u$  is the zonal wind speed;  $v$  is the meridional wind speed;  $\xi$  is the mass or number concentration of aerosols and chemical species, at the near-surface. The variabilities of convective updrafts at the near-surface are modulated by non-organized turbulence and mesoscale organized flow driven by cold pools. UNICON (and stochastic UNICON) parameterizes cold pools by solving prognostic equations for the net fractional area and mean conservative scalars of cold pools. The perturbation of convective updrafts by mesoscale organization  $\Delta\phi_\Omega$  is computed using the prognosed cold pool properties, and mesoscale organization parameter  $\Omega$ , which represents the strength of mesoscale organization, is computed as a linear function of the net cold pool area.

The distribution of thermodynamic scalars is assumed as a multivariate Gaussian with the constraint of  $w > 0$ . The total standard deviation of thermodynamic scalar  $\sigma_\phi^*$  is parameterized as

$$\sigma_\phi^* = \sqrt{c_1\sigma_\phi^2 + c_2(\Delta\phi_\Omega)^2}, \quad (1)$$

where  $\sigma_\phi$  is the standard deviation of  $\phi$  derived from the surface-layer similarity theory and  $c_1$  and  $c_2$  are tunable parameters. The parameterization is based on the assumption that the variance of each thermodynamic variable is the sum of variances from non-organized turbulence and mesoscale organized flow. The final thermodynamic properties of convective updrafts at the near-surface are derived as

$$\hat{\phi} = \sigma_\phi^* \alpha_\phi + \bar{\phi}_s, \quad (2)$$

where  $\bar{\phi}_s$  is the grid-mean value of  $\phi$  at the surface and  $\alpha_\phi$  is a random sample from a standard multivariate Gaussian where the inter-variable correlations are derived from the surface-layer similarity theory. The hat denotes the mean updraft property.

The parameterization of the distribution of updraft radius is based on the observations from the previous studies, where the number density of cloud horizontal size follows a power-law distribution with a scale break (Heus & Seifert, 2013; Neggers et al., 2003; O'Brien et al., 2013; Wood & Field, 2011). The number density PDF of updraft radius at the near-surface  $P_n$  is parameterized as

$$P_n(\hat{x})/N = a_1 \hat{x}^{-2-\hat{x}^{1.7}}, \quad \int_0^\infty (P_n(\hat{x})/N) d\hat{x} = 1, \quad (3)$$

where  $\hat{x} = \hat{R}/R_b$  is the updraft plume radius  $\hat{R}$  normalized by the scale break radius  $R_b$ ,  $N$  is the total updraft number density in the unit of  $[\# \text{ m}^{-2}]$ , and  $a_1$  is a normalization constant. The scale break radius  $R_b$  determines the maximum cloud size in a model grid, and there are some evidences that the scale break radius is largely increased by mesoscale organization (e.g., Neggers et al., 2019). We parameterize the scale break radius as a linear function of the mesoscale organization parameter  $\Omega$ :

$$R_b = R_b|_{\Omega=0} + (R_b|_{\Omega=1} - R_b|_{\Omega=0})\Omega, \quad (4)$$

where  $R_b|_{\Omega=0}$  and  $R_b|_{\Omega=1}$  are  $R_b$  at  $\Omega = 0$  and  $\Omega = 1$ , respectively. The detailed derivation and validation of the proposed parameterization are available in SP20 and SB23.

**Table 1**  
*Parameters and Their Values Used in the Global Simulation With Stochastic UNICON*

Parameter	Value	Description
$c_1$	0.9	Scaling factor for the variance from non-organized turbulence (Equation 1)
$c_2$	0.5	Scaling factor for the variance from mesoscale organized flow (Equation 1)
$R_b _{\Omega=0}$	110 m	Scale break radius at the near-surface at $\Omega = 0$ (Equation 4)
$R_b _{\Omega=1}$	3,500 m (ocean), 9,000 m (land)	Scale break radius at the near-surface at $\Omega = 1$ (Equation 4)
$c_{at}$	$4.0 \times 10^{-3} \text{ m}^{-1}$ (land)	Autoconversion efficiency over land; Originally $2.0 \times 10^{-3} \text{ m}^{-1}$ in UNICON
$\hat{q}_{c,\text{crit}}$	$5.0 \times 10^{-4} \text{ kg kg}^{-1}$ (land)	Critical in-cumulus liquid water content for the formation of precipitation over land; Originally $6.0 \times 10^{-4} \text{ kg kg}^{-1}$ in UNICON

*Note.* The parameters that are newly added or have different values from UNICON are listed.

Stochastic UNICON can be configured with various methods to sample convective updrafts from the joint PDF. In this study, we will use a Monte-Carlo method to sample convective updrafts from the joint PDF, as in SB23. Each sampled updraft has a fractional area of  $\hat{a} = \hat{A}_s/n_s$ , where  $\hat{A}_s$  is the total updraft fractional area at the near-surface and  $n_s$  is the number of updrafts to be sampled ( $n_s = 5$  is used in this study). The value of  $n_s = 5$  is determined in SB23 using SCM tests as a trade-off between the model performance and computational cost. Table 1 lists the parameters and their values used in stochastic UNICON.  $c_1$ ,  $c_2$ ,  $R_b|_{\Omega=0}$ , and  $R_b|_{\Omega=1}$  are the tunable parameters newly introduced in stochastic UNICON (Equations 1 and 4). The values of  $c_1$ ,  $c_2$ , and  $R_b|_{\Omega=0}$  are set by rounding the values that were calibrated using a SCM in SB23. The value of  $R_b|_{\Omega=1}$  over the ocean is changed from the SCM-calibrated value of 2,190 m to 3,500 m in order to balance the global energy budget. In addition, the values of parameters related to the autoconversion process in cumulus ( $c_{at}$  and  $\hat{q}_{c,\text{crit}}$ ) over land are modified, to match the mean precipitation over land.

## 2.2. Model Experiments

The atmospheric GCM (AGCM) used in this study is SAM0-UNICON (Park et al., 2019). SAM0-UNICON uses the same dynamic core and physics parameterizations as CAM5, except for shallow and deep convection and macrophysics schemes. The finite volume dynamic core (Lin & Rood, 1996), the double-moment stratiform microphysics scheme of Morrison and Gettelman (2008), the Rapid Radiative Transfer Method for GCMs radiation scheme (Iacono et al., 2008; Pincus et al., 2003), the planetary boundary layer (PBL) scheme of Bretherton and Park (2009), and the aerosol conversion scheme of X. Liu et al. (2012) are the identical components with CAM5. The macrophysics of Park et al. (2014) in CAM5 is modified to include detrained cumulus (Park et al., 2017). Finally, UNICON replaces shallow and deep convection schemes in CAM5, which parameterizes all subgrid dry and moist convection.

We ran two global climate simulations, one with UNICON and the other with stochastic UNICON, with a horizontal resolution of  $0.9^\circ \times 1.25^\circ$ , 30 vertical levels, a model physics time step of  $\Delta t = 1,800$  s, and a dynamics time step of  $\Delta t = 225$  s. Hereinafter, the two simulations are referred to as UNICON and UNICON-STO, respectively. The simulations are conducted for 36 years, from January 1979 to December 2014, according to the Atmospheric Model Intercomparison Project (AMIP) configuration described in the CMIP6 experiments specification (Eyring et al., 2016). The historical climate forcing data are prescribed as described in Park et al. (2019), so the simulations include climate change signals. Following the AMIP configuration, the observed sea surface temperature and sea ice fraction are prescribed, and a land model (Community Land Model version 4; CLM4) is coupled to simulate land surface states. The simulations are initialized from the atmosphere and land states on 1 January 1979 obtained from the historical coupled simulation of SAM0-UNICON. The computational cost of the simulation of stochastic UNICON increases by 19% compared to that of UNICON when it is run with 1,088 cores in a parallel processing system.

## 2.3. MJO Diagnostics and MJO Precipitation Budget

We use the CLIVAR MJO Working Group diagnostics package (Waliser et al., 2009) to obtain diverse MJO diagnostics. Daily anomalies are obtained by removing the mean and first three harmonics of the annual cycle

over the 1979–2014 period. Then, the anomalies are bandpass-filtered using a 101-point Lanczos filter to extract the intraseasonal anomalies within 20–100 day time scales. The MJO phase composites are computed using the real-time multivariate MJO index (RMM index; Wheeler & Hendon, 2004), defined as the first two principal components of intraseasonal daily anomalies of outgoing longwave radiation (OLR), and 850 and 200 hPa zonal winds averaged over 15°S–15°N.

To understand the characteristics of MJO propagation in the global simulations, a precipitation budget analysis of Adames (2017) is conducted. The precipitation budget is a variant of the moisture budget where the inverse of the convective moisture adjustment time scale is weighted in each term to account for the moisture–precipitation relationship. The vertically integrated moisture budget equation can be written as follows:

$$\frac{\partial \langle q \rangle'}{\partial t} = -\left\langle u \frac{\partial q}{\partial x} \right\rangle' - \left\langle v \frac{\partial q}{\partial y} \right\rangle' + E' + C', \quad (5)$$

$$C' = -\left\langle \omega \frac{\partial q}{\partial p} \right\rangle' - P', \quad (6)$$

where  $q$  is the specific humidity,  $u$  and  $v$  are the zonal and meridional wind speeds, respectively, and  $\omega$  is the vertical pressure velocity;  $P$  and  $E$  are the precipitation and surface evaporation, respectively. The angle brackets indicate the mass-weighted vertical integral from the surface to 100 hPa, and the prime symbol denotes the intraseasonal (20–100 days band-filtered) anomalies. The term  $C$  denotes the convectively driven column process, which is the sum of the vertical advection of moisture and the precipitation.

The relationship between moisture and precipitation over the tropical ocean is hypothesized as a nonlinear relationship (Bretherton et al., 2004), and it can be approximated in the following form:

$$P(R_h) = P_0 \exp(aR_h), \quad (7)$$

where  $R_h = \langle q \rangle / \langle q_s \rangle$  is the column relative humidity (CRH),  $q_s$  is the saturation specific humidity, and  $P_0$  and  $a$  are constants. The values of  $P_0$  and  $a$  are determined from observational data and the two simulations (see Section 3.3). By linearizing Equation 7, the anomalous precipitation can be linked with the anomalous moisture:

$$P' \cong \frac{\langle q \rangle'}{\tau_c}, \quad \bar{\tau}_c = \frac{\langle \bar{q}_s \rangle}{aP}, \quad (8)$$

where  $\tau_c$  is the convective moisture adjustment time scale and the overbar denotes a 100-day low-pass filtered field.  $\tau_c$  is analogous to the adjustment time scale in the simplified Betts–Miller convective adjustment scheme (Betts & Miller, 1986; Frierson, 2007), and it determines the strength of the conversion of moisture anomaly to precipitation. Finally, the budget equation for the precipitation anomaly can be written as

$$\frac{\partial P'}{\partial t} = -\frac{1}{\tau_c} \left\langle u \frac{\partial q}{\partial x} \right\rangle' - \frac{1}{\tau_c} \left\langle v \frac{\partial q}{\partial y} \right\rangle' + \frac{E'}{\tau_c} + \frac{C'}{\tau_c}. \quad (9)$$

## 2.4. Observational Data

For the evaluation of the model mean climates, the following datasets are used: the Clouds and the Earth's Radiant Energy System Energy Balanced and Filled (CERES-EBAF; Loeb et al., 2009) for shortwave and longwave cloud radiative forcing; the European Centre for Medium-Range Weather Forecasts (ECMWF) Interim Reanalysis (ERA5; Simmons et al., 2007) for temperature, relative humidity, sea level pressure, and zonal wind; the European Remote Sensing Satellite Scatterometer (ERS; Bentamy et al., 1999) for ocean surface wind stress; the Willmott–Matsuura (Willmott; Willmott & Matsuura, 1995) data for land surface air temperature; the Global Precipitation Climatology Project (GPCP) monthly product version 2.1 (Adler et al., 2003) for global precipitation rate. These datasets are interpolated onto the native model grid to obtain mean climate diagnostics.

For the MJO diagnostics and precipitation budget analysis, the following datasets are used. We use the National Oceanic and Atmospheric Administration daily interpolated OLR product (Liebmann & Smith, 1996) and daily averaged precipitation rate from the Tropical Rainfall Measuring Mission 3B42 version 7 (TRMM 3B42v7;

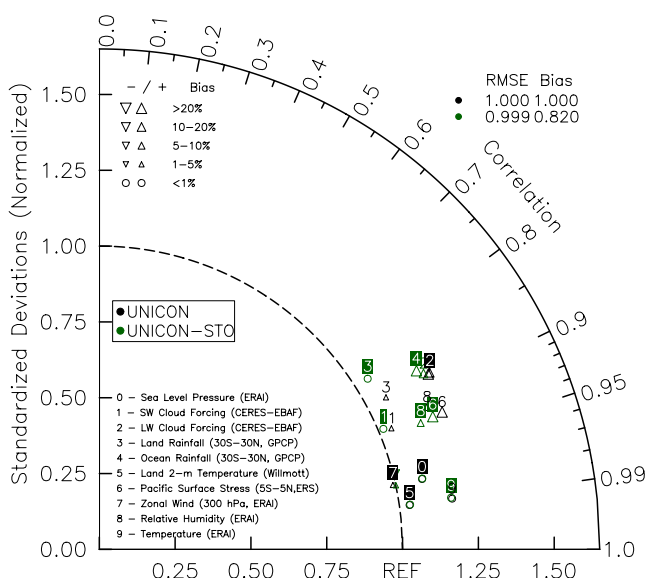


**Figure 1.** A space-time Taylor diagram from the UNICON (black) and UNICON-STO (green) simulations. Using the monthly climatology for all the available grid points, the correlations with the observation and the standardized deviations normalized by observed standard deviation are computed for 10 climate variables indicated on the lower-left portion of the figure. The denoted RMSE (bias) is the average of the RMSE (bias) of a simulated individual variable divided by the average RMSE (bias) of UNICON.

STO both overestimate standardized deviations of the majority of the climate variables, UNICON-STO reduces standardized deviations of SWCF, ocean and land rainfall, Pacific surface stress, and relative humidity. The correlations with observations are quite similar in UNICON and UNICON-STO and show different trends between variables; for instance, the correlation of land rainfall is reduced ( $0.883 \rightarrow 0.844$ ) and relative humidity is increased ( $0.917 \rightarrow 0.931$ ) from UNICON to UNICON-STO. The result shows that general performances on simulating spatio-temporal patterns are very similar in UNICON and UNICON-STO, but stochastic UNICON slightly improves the model performance in terms of mean bias and variance.

The model performance with stochastic UNICON can be improved with more careful calibration of the model parameters. In SB23, the tunable parameters in stochastic UNICON are calibrated using various SCM cases over the ocean. Then, the parameters over land are determined from the multiple global simulations with manually adjusted parameters. However, inferred from the reduced correlation of land rainfall in UNICON-STO, there is a possibility that the land parameters are not calibrated properly. In addition, extending the bulk plume to the spectral/stochastic plume model might require adjusting mixing and rain production processes since the characteristics of the bulk plume and individual plumes are different.

Figure 2 shows the global climatology of surface precipitation rate from the GPCP observation and the model biases. Both simulations produce higher mean precipitation than the observation, exhibiting distinct positive precipitation biases over the intertropical convergence zone (ITCZ) and South Pacific convergence zone. UNICON-STO reduces the mean bias of precipitation in UNICON by  $0.04 \text{ mm day}^{-1}$ , while the RMSE is increased by  $0.02 \text{ mm day}^{-1}$ . The precipitation biases are weakened over the western Indian Ocean, ITCZ, and western equatorial Atlantic in UNICON-STO. However, the magnitudes of positive bias over the northwestern Pacific and negative bias over the Maritime Continent are intensified. The precipitation biases over the Maritime Continent and northwestern Pacific appear to be negatively correlated, as indicated in other GCM simulations (e.g., Schiemann et al., 2014). Schiemann et al. (2014) demonstrated that the decrease in precipitation over the Maritime Continent is associated with the weakening of the Walker circulation and the decreased moisture convergence, which lead to an increase in precipitation over the northwestern Pacific. Indeed, UNICON-STO exhibits decreases in large-scale vertical velocities over the Maritime continent and increases over the northwestern Pacific relative to

G. Huffman et al., 2007) product. Various atmospheric state variables are obtained from the fifth generation of the ECMWF reanalysis (ERA5) product (Hersbach et al., 2020). The hourly ERA5 data are averaged daily. The atmospheric field variables that are used in the precipitation budget analysis are obtained at 27 pressure levels between 1,000 and 100 hPa. OLR and ERA5 data are obtained for the period 1979–2014, and precipitation data are obtained for the period 1998–2014. All observational data and model outputs for the MJO diagnostics and budget analysis are interpolated onto a  $2.5^\circ \times 2.5^\circ$  horizontal grid using areal conservative remapping. Note that ERAI is used for the mean state evaluation, while the most updated ECMWF reanalysis (ERA5) is used for the evaluation of the MJO. We used ERAI for the mean state evaluation in order to consistently compare model performances with previous versions.

## 3. Results

### 3.1. Mean State

Figure 1 is a Taylor diagram (Taylor, 2001) summarizing the model performance in reproducing the observed global mean climate. The mean RMSEs of the two simulations are similar; however, UNICON-STO exhibits an 18% smaller mean bias compared to UNICON. More than 10% of biases are reduced from UNICON to UNICON-STO for shortwave cloud forcing (SWCF), land rainfall, Pacific surface stress, and relative humidity (Table S1 in Supporting Information S1). Specifically, the negative mean SWCF bias in UNICON is alleviated in UNICON-STO, consistent with the decreased low cloud fraction in UNICON-STO (global mean low cloud fraction is 41.73% in UNICON and 40.14% in UNICON-STO). While UNICON and UNICON-

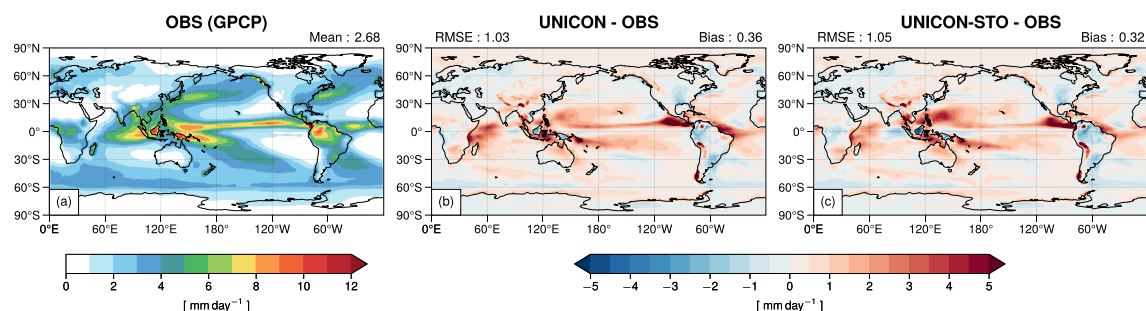


**Figure 2.** Annual surface precipitation rate from (a) the Global Precipitation Climatology Project observation and the biases compared to the observations from (b) UNICON and (c) UNICON-STO. The global mean of the observation or the mean bias of the simulation is shown at the top right of each plot, and the RMSE of the simulation is shown at the top left of each plot.

UNICON (Figures S2e and S2f in Supporting Information S1), showing the weakening of the circulation. Since the Maritime Continent exerts significant impacts on the modulation of the MJO and other large-scale tropical variabilities (Neale & Slingo, 2003; S. Yang et al., 2019), a detailed investigation of the bias is required.

The first row of Figure 3 shows the annual zonal-mean updraft mass flux of UNICON and UNICON-STO. The two simulations show substantially different updraft mass flux profiles, where UNICON-STO presents a much stronger mass flux below the height of 800 hPa, and the height of mass flux maximum is lowered (Figure 3a). This indicates more frequent shallow convection due to the spectral representation of stochastic UNICON, as demonstrated in SB23. However, it is not confirmed that the increased low-level mass flux in UNICON-STO is more consistent with observations. The simulated mass flux profile needs to be evaluated against observations or cloud-resolving model simulations with a consistent definition of convective updrafts. The second row of Figure 3 shows the annual zonal-mean relative humidity of the ERAI observation and the model biases. Both

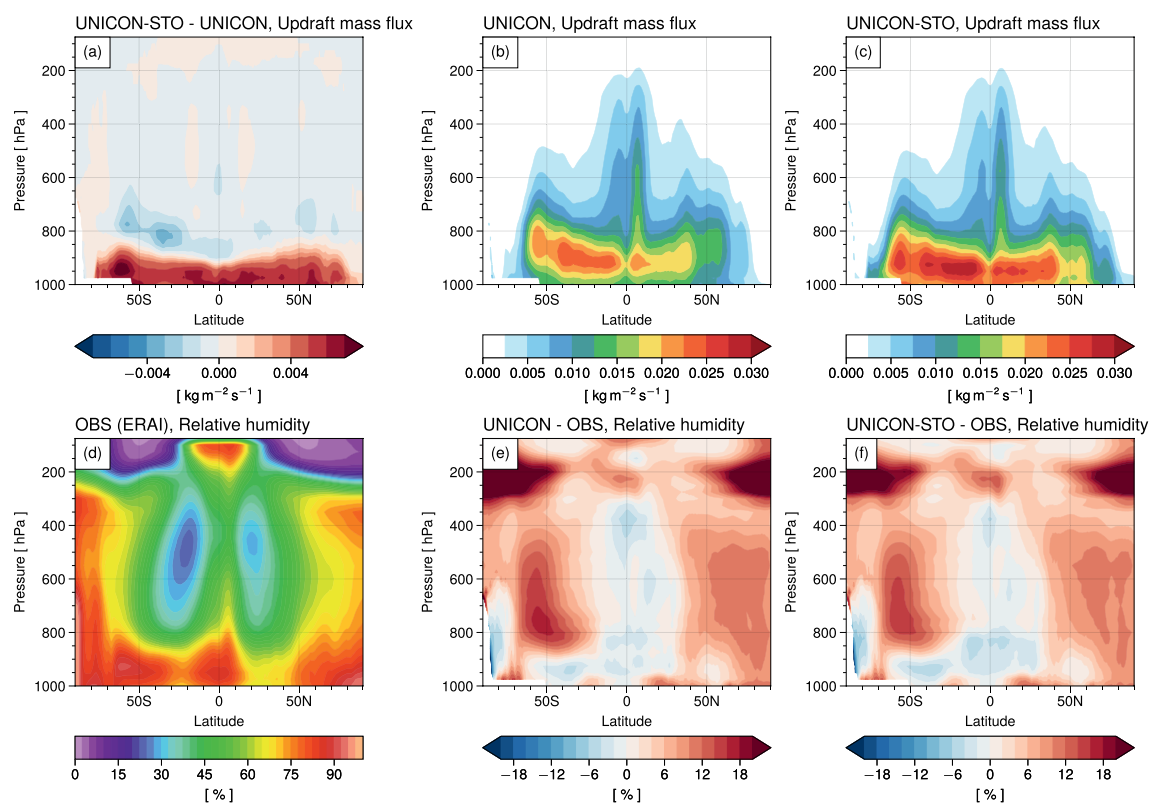


**Figure 3.** Annual zonal-mean vertical cross sections of updraft mass flux from (b) UNICON and (c) UNICON-STO and (a) the updraft mass flux difference between the two simulations (UNICON-STO minus UNICON); relative humidity from (d) the ERAI observation and the biases compared to the observation from (e) UNICON and (f) UNICON-STO.

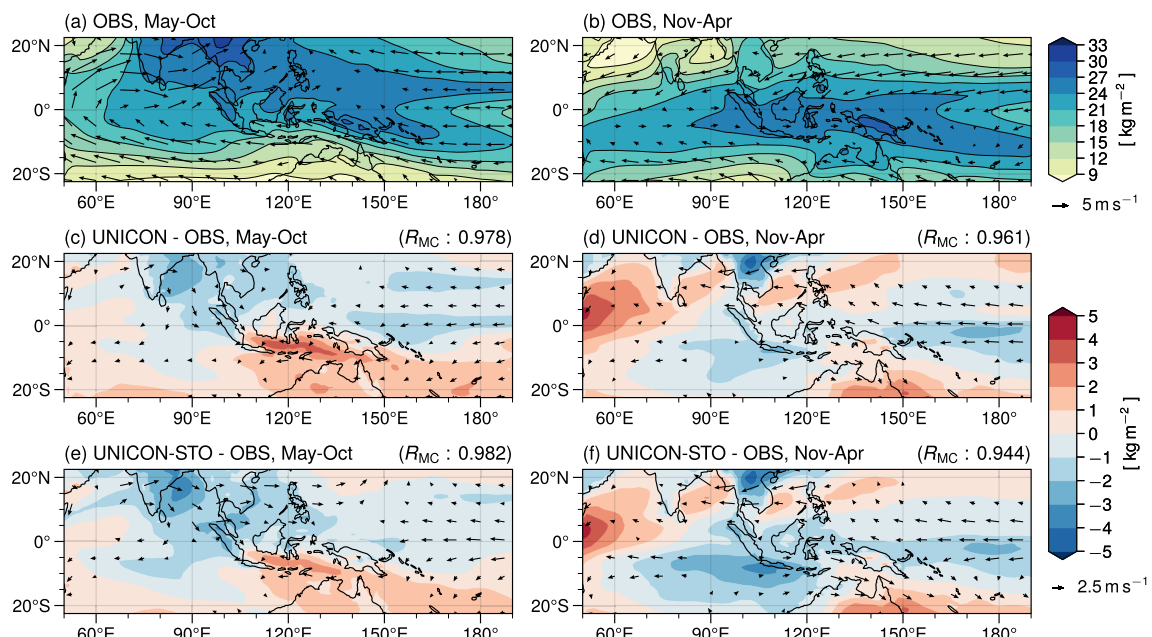


**Figure 4.** 650–900 hPa integrated specific humidity (shading) and wind vectors at 850 hPa from (a and b) the ERAI observation and the biases compared to the observation from (c and d) UNICON and (e and f) UNICON-STO, during May–October (left column) and November–April (right column).  $R_{MC}$  denotes the pattern correlation of lower-tropospheric moisture between the observation and simulation in the area near the Maritime Continent ( $20^{\circ}\text{S}$ – $20^{\circ}\text{N}$ ,  $90^{\circ}$ – $135^{\circ}\text{E}$ ).

simulations exhibit strong positive relative humidity biases in the extratropics and relatively smaller negative biases in the tropics. UNICON-STO slightly reduces the positive biases in mid-high latitudes and negative biases in levels above 600 hPa over the tropics. The increase of relative humidity in the upper troposphere over the tropics is contributed by the anomalous cooling and moistening by convective processes in UNICON-STO relative to UNICON (Figures S1b and S1d in Supporting Information S1). UNICON-STO produces anomalous heating below 900 hPa and anomalous cooling in 800–900 hPa levels by convective processes relative to UNICON (Figures S1b and S1d in Supporting Information S1). The anomalous convective tendencies destabilize the lower troposphere and contribute decrease in low cloud fraction. In addition, the decrease in relative humidity may contribute to reducing the SWCF bias, while considerable relative humidity errors remain in UNICON-STO.

Before discussing the MJO diagnostics, we examine the simulated mean states that are closely related to MJO characteristics during boreal summer (May–October) and winter (November–April). Several studies have shown that GCMs with relatively good MJO simulation skills tend to have higher mean state moisture gradients in the lower free troposphere around the Maritime Continent area (Ahn et al., 2020; Gonzalez & Jiang, 2017; Jiang, 2017). Figure 4 shows the observation and model biases of lower-tropospheric moisture and 850 hPa wind vectors in the two seasons. In both simulations, the lower-tropospheric moisture is underestimated where the observed moisture maximum is located and overestimated in surrounding areas. Therefore, the meridional moisture gradients are underestimated in the two simulations during both seasons. The mean moisture patterns of the two simulations are similar, but some noticeable differences exist. Especially during winter, UNICON-STO shows a stronger negative bias over the southern part of the eastern equatorial Indian Ocean compared to UNICON. The stronger negative bias is related to the stronger anomalous divergent flow near this region (Figure 4f). Following Gonzalez and Jiang (2017), we calculate the pattern correlation of lower-tropospheric moisture between the observation and simulation in the area near the Maritime Continent, which is known to be well correlated with the MJO propagation simulation skill. The pattern correlation of the two simulations during summer is similar, but UNICON-STO shows a substantially lower correlation than UNICON during winter.

### 3.2. MJO Diagnostics

Figure 5 shows the wavenumber-frequency spectra of OLR and 850 hPa zonal wind from the observations and simulations. Compared to the observations, the two simulations both produce much stronger power in a wide frequency domain during summer. UNICON and UNICON-STO reproduce the observed MJO peak in

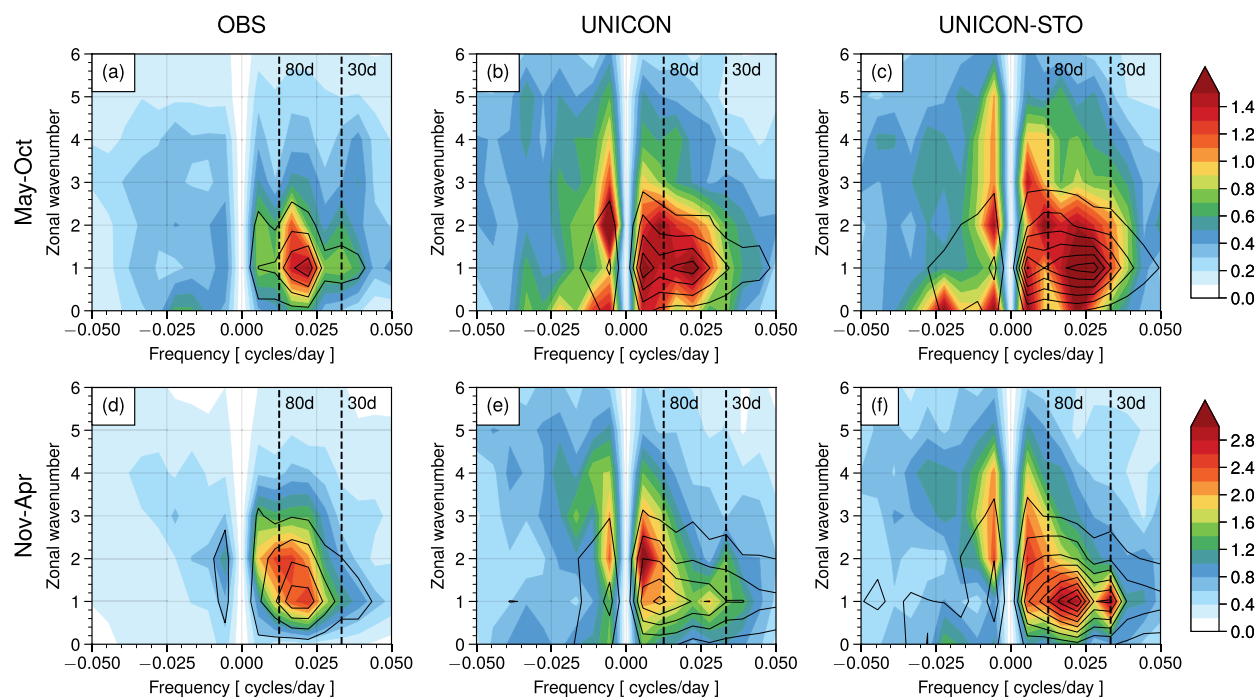


**Figure 5.** Wavenumber-frequency spectra of outgoing longwave radiation (shading;  $\text{W}^2 \text{ m}^{-4}$ ) and 850 hPa zonal wind (contour;  $0.02 \text{ m}^2 \text{ s}^{-2}$  intervals) averaged over  $10^\circ\text{S}$ – $10^\circ\text{N}$  during summer (May–October; first row) and winter (November–April; second row) for (a and d) the observations, (b and e) UNICON, and (c and f) UNICON-STO.

30–80-day periods with zonal wavenumbers 1–2 during summer. However, UNICON produces a power peak stronger than the MJO peak in periods greater than 80 days, while the dominant variability of UNICON-STO is in the 30–80 days range. During winter, UNICON simulates a variability that is too strong in the low-frequency regime and a weaker MJO power (Figure 5e). In contrast, UNICON-STO simulates the adequate power of winter MJO (Figure 5f). During both summer and winter, UNICON and UNICON-STO overestimate variabilities in low-frequency regimes in westward and eastward directions. UNICON-STO shows substantially larger MJO-related variabilities than the observations for OLR during summer and for 850 hPa zonal wind during both seasons.

Figure 6 is the result of a cross-spectrum analysis, showing coherence squared between OLR and 850 hPa zonal wind. The same figure with a larger wavenumber-frequency domain is available as Figure S3 in Supporting Information S1. The observations display high coherence squared (peaking at greater than 0.6) between OLR and 850 hPa zonal wind in periods of 20–80 days with zonal wavenumbers 1–2, indicating a strong coupling between large-scale circulation and convection in the MJO. UNICON shows a coherence squared peak for the simulated MJO but 15–30% smaller values relative to the observations. Still, UNICON indicates much larger coherence than that of CAM5 (Park et al., 2019). UNICON-STO shows noticeably larger coherence related to the MJO than UNICON, especially for zonal wavenumber 1. Both UNICON and UNICON-STO show a lack of coherency between OLR and zonal wind in a zonal wavenumber of 2 (2 cycles along the circumference). Stochastic UNICON also improves the simulation of other equatorial waves. UNICON-STO does a better job of reproducing coherences of slow Kelvin waves (periods of 8–20 days) with zonal wavenumbers greater than 5 and  $n = 1$  equatorial Rossby waves.

The multivariate empirical orthogonal function (EOF) patterns of intraseasonal OLR and 850 and 200 hPa zonal winds (Figure S4 in Supporting Information S1), which are used to calculate the RMM index, confirm the low coherency between convection and wind for zonal wavenumber 2 in UNICON and UNICON-STO. The sign and order of the EOF1 and EOF2 in the simulations are adjusted to match the observations. In the observations, EOF1 shows a sharp peak of negative OLR and steep changes in zonal winds near  $90^\circ\text{E}$ . Note that the observed EOFs are slightly different from Wheeler and Hendon (2004) since different datasets and periods are used and also the data are bandpass-filtered in this study. In contrast to the observations, the peaks of OLR and zonal winds EOFs

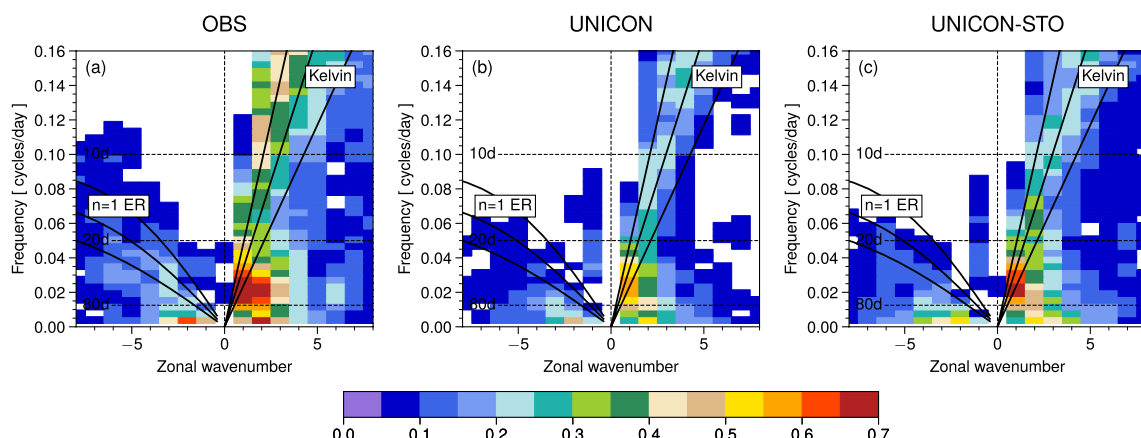


**Figure 6.** Symmetric component of coherence squared between daily anomalies of outgoing longwave radiation and 850 hPa zonal wind averaged over 15°S–15°N from (a) the observations, (b) UNICON, and (c) UNICON-STO. The dispersion curves for Kelvin and  $n = 1$  equatorial Rossby waves are shown.

in the simulations are much broader, especially for EOF1. The EOF patterns of the simulations are more like sine waves with zonal wavenumber 1. The EOF structures of UNICON and UNICON-STO are almost identical. However, the total variances of EOF modes in UNICON-STO (EOF1: 17.9%, EOF2: 21.5%) are higher than in UNICON (EOF1: 15.1%, EOF2: 18.4%), which better matches with the observations (EOF1: 22.2%, EOF2: 21.9%).

Figure 7 shows lag-longitude diagrams of intraseasonal precipitation (shading) and 850 hPa zonal wind (contour) correlated against precipitation at an Indian Ocean reference area. The figure is plotted for the period of 1998–2014 when the TRMM data set is available. The observations show the eastward propagation of precipitation anomalies and associated wind convergence across the Eastern Hemisphere with a phase speed of about  $4 \text{ m s}^{-1}$ . The lag between zonal wind anomalies and precipitation anomalies is about 5–7 days. During summer, both UNICON and UNICON-STO reproduce the observed eastward propagation of precipitation and zonal wind anomalies. However, during winter, UNICON substantially underestimates the eastward propagation of precipitation

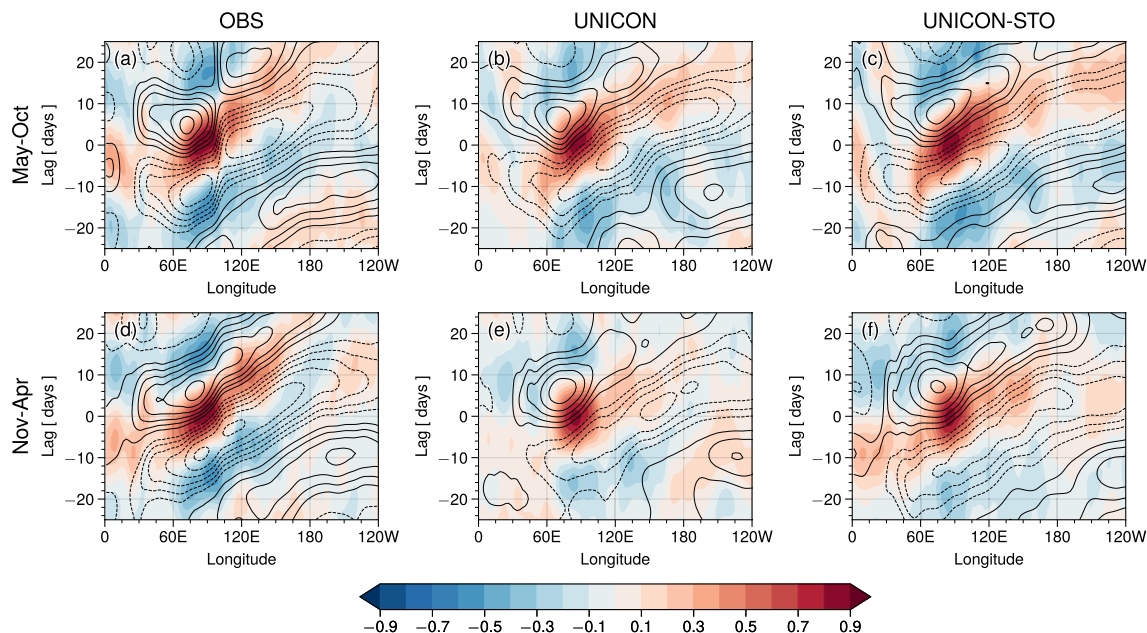


**Figure 7.** Lead-lag correlations of the 20–100-day bandpass-filtered daily precipitation (shading) and 850 hPa zonal wind (contour; 0.1 intervals) correlated to the daily time series of bandpass-filtered precipitation averaged in the area over the Indian Ocean (10°S–10°N, 80°–100°E) as a function of longitude during summer (May–October; first row) and winter (November–April; second row) of 1998–2014, from (a and d) the observations, (b and e) UNICON, and (c and f) UNICON-STO.

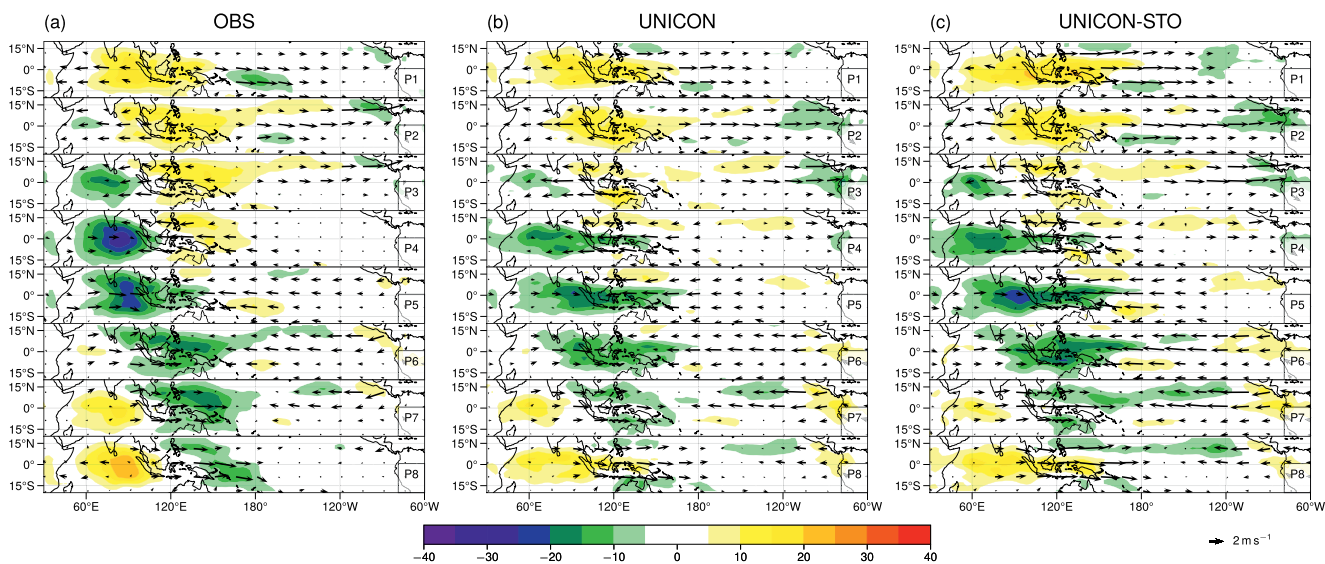


**Figure 8.** Composite of the 20–100-day bandpass-filtered daily anomalies of outgoing longwave radiation (shading;  $\text{W m}^{-2}$ ) and wind vectors at 850 hPa as a function of RMM phase during November–April from (a) the observations, (b) UNICON, and (c) UNICON-STO.

across the Maritime Continent and western equatorial Pacific and associated wind convergence. UNICON-STO simulates more realistic propagation of precipitation and zonal wind anomalies during winter. The observations show an abrupt decrease of correlation (especially 850 hPa zonal wind) at about 110°E due to the barrier effect of the Maritime Continent during summer, when a large portion of MJO events passes through Sumatra (Hsu & Lee, 2005; C. Zhang & Ling, 2017). The barrier effect is weaker in winter since the MJO detours the Maritime Continent (Kim et al., 2017). UNICON and UNICON-STO do not show an abrupt correlation decrease during summer. The main convection activities in the simulations are biased southward compared to the observation during summer (as indicated in Figure S2 of Supporting Information S1), so the simulated MJO events might be less affected by the barrier effect. Further analysis with MJO tracking is needed to confirm the reduced barrier effect. The lag-latitude diagrams (Figure S5 in Supporting Information S1) indicate that both simulations reproduce the observed northward propagation of the MJO during summer and southward propagation during winter. UNICON-STO better reproduces the observed correlation associated with northward propagation during summer, but during winter, UNICON-STO shows too elongated correlation pattern of precipitation in the southward direction.

The simulated composite life cycles of intraseasonal anomalies of OLR and 850 hPa wind vectors during winter are examined (Figure 8 and Figure S6 in Supporting Information S1). The model composite plots are constructed by projecting bandpass-filtered daily anomalies onto the model EOF patterns. UNICON simulates substantially weaker deep convection over the Indian Ocean and the western equatorial Pacific where the convection passed through the Maritime Continent during winter (Figure 8). UNICON-STO noticeably improves the simulation of the life cycle of the winter MJO, simulating stronger MJO-related OLR anomalies. The convection activity after passing through the Maritime Continent is more strongly maintained in UNICON-STO. Nevertheless, the two simulations exhibit too strong wind anomalies over the equatorial Pacific, as indicated by large EOF amplitudes of zonal winds over the Pacific (Figure S4 in Supporting Information S1).

Here, we discuss the relationship between the simulated mean state and MJO characteristics. The reason why summer MJO is stronger than winter MJO in the simulations can be partially explained by the fact that the simulations show smaller moisture mean state bias during summer (Figure 4). The negative moisture bias near the Maritime Continent region during winter can suppress the simulated MJO activity. Comparing the two simulations, the mean state differences exhibit contrasting impacts on the MJO simulation performance. There are some regional mean state differences that may contribute to the improvement of the MJO in UNICON-STO. In summer, the intensity of Indian summer monsoon westerlies is stronger in UNICON-STO than in UNICON (Figures 4c and 4e). It can contribute to the enhancement of MJO eastward propagation, as the advection of anomalous moisture by mean zonal wind is important during summer (Adames et al., 2016). In winter, the meridional moisture

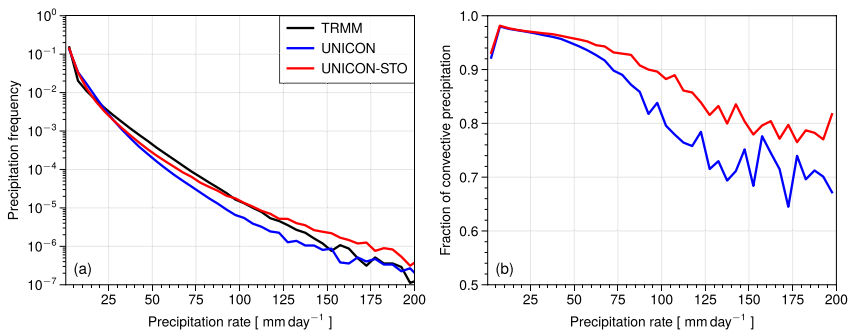


**Figure 9.** (a) Frequency spectra and (b) fraction of convective precipitation as a function of daily surface precipitation rate in the tropical region (15°S–15°N), obtained from UNICON and UNICON-STO. In (a), the frequency spectra of the TRMM 3B42v7 daily precipitation are also shown.

gradient is steeper in UNICON-STO to the south of the equator around 100°–120°E (Figures 4d and 4f). Ahn et al. (2020) and Kang et al. (2020) found that models with higher moisture gradients in the same area tended to simulate the eastward propagation of the MJO better. In contrast, the lower moisture pattern correlation in UNICON-STO during winter indicates a negative impact on the MJO simulation performance, so the prominent MJO enhancement in UNICON-STO during winter is not explained. The result implies that the mean state difference is not sufficient to explain the difference in the MJO characteristics between the two simulations.

### 3.3. Precipitation Budget Analysis

Before demonstrating the result of the precipitation budget analysis, we discuss the simulated characteristics of precipitation and their relation to water vapor. Figure 9 shows frequency spectra and the fraction of convective precipitation as a function of the daily surface precipitation rate over the tropics. UNICON-STO generally increases the frequency of intense precipitation greater than 25 mm day<sup>-1</sup> with respect to UNICON. The simulated frequencies in UNICON-STO are more consistent with the TRMM observation than those in UNICON, while UNICON already simulates realistic precipitation frequency spectra. The increased frequency of heavy rainfall is related to the increase in the fraction of convective precipitation in UNICON-STO (Figure 9b). Over 95% of moderate-intensity rainfall is convective precipitation (from the convection schemes) in the simulations, and the ratio of convective precipitation decreases as precipitation intensity increases. UNICON-STO increases up to 10% of convective precipitation fraction for intense precipitation greater than 25 mm day<sup>-1</sup>.

The observed and simulated relationships between CRH ( $R_h$ ) and precipitation ( $P$ ) are displayed in Figure 10. The data are obtained from the warm pool region where Adames (2017) determined the value of  $a$  in Equation 7. The first row of the figure shows the density plots of  $R_h$  and precipitation and nonlinear least squares fits of data on Equation 7. It is clear that the relationship between the two variables is exponential in the observation and simulations, while there are considerable uncertainties. The noticeable deficiency of the model simulations is the overestimation of precipitation intensity at low  $R_h$ . For  $R_h = 0.7 \sim 0.75$ , the simulations tend to produce light-to-moderate rain rates ( $P = 5 \sim 20$  mm day<sup>-1</sup>) too frequently, and for  $R_h > 0.75$ , the simulations underestimate the frequency of very light rain rates ( $P < 5$  mm day<sup>-1</sup>). Rushley et al. (2018) demonstrated that many CMIP5 models have the same issue of early precipitation pickup on a drier regime. This shows the problem of most GCMs where their convection schemes are insensitive to environmental humidity (Derbyshire et al., 2004).

The values of  $a$  determined in Figure 10 are used to calculate the precipitation budget for the observation and simulations. The fitted value of  $a = 13.95$  from the TRMM data set is in the range of the values obtained from other studies, 15.6 from Bretherton et al. (2004), 12.1 from Adames (2017), and 14.72 from Rushley et al. (2018). In UNICON,  $a$  is measured as a smaller value of 9.67, while  $a$  is measured as 11.55 in UNICON-STO, showing a value in between the observation and UNICON. The larger value of  $a$  in UNICON-STO is largely contributed by increased intense precipitation in the high  $R_h$  regime (Figure 10c). The increased density for high  $R_h$  and  $P$  implies that UNICON-STO simulates stronger organized convection (e.g., Adames, 2017). The corresponding mean convective adjustment time scales ( $\bar{\tau}_c$ ) computed with Equation 8 (using the climatological mean of precipitation rate and vertically-integrated saturation specific humidity) over the warm pool region are 17.0, 25.1,

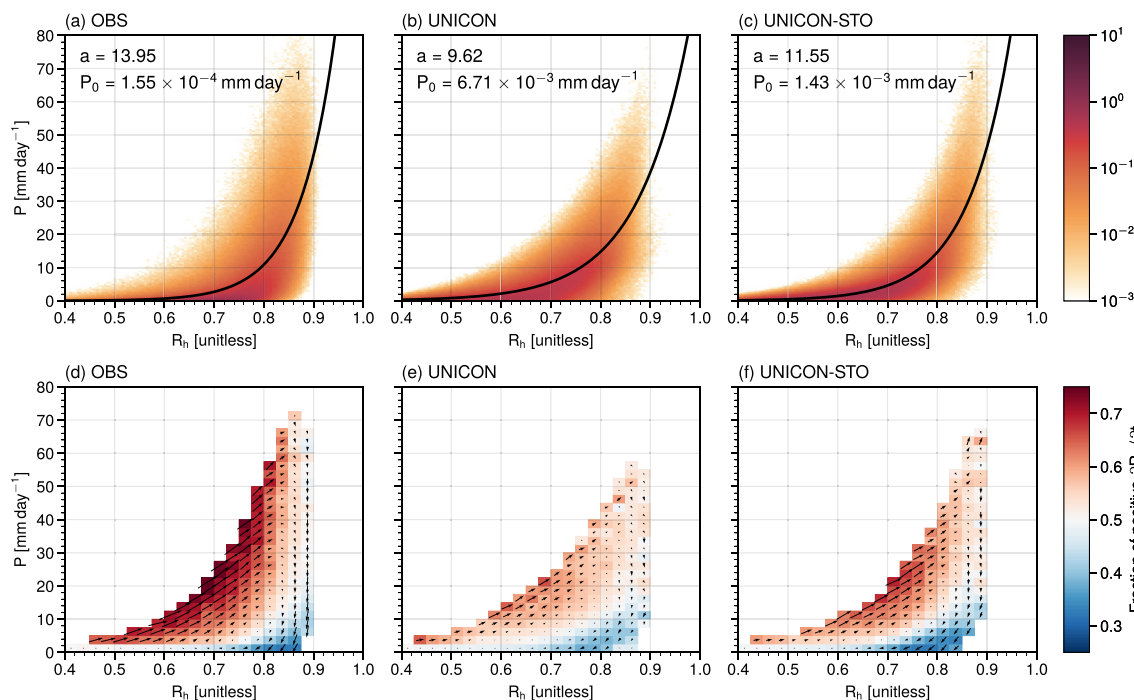


**Figure 10.** Panels in the first-row show the density plots of daily precipitation versus column relative humidity ( $R_h$ ) from the (a) TRMM and ERA5 observations, (b) UNICON, and (c) UNICON-STO. The black line denotes the nonlinear least squares fit of the data in Equation 7. Panels in the second-row show tendencies of  $R_h$  and precipitation as vectors and fraction of positive  $R_h$  tendency as color shading, where the data are obtained from the (d) TRMM and ERA5 observations, (e) UNICON, and (f) UNICON-STO. The vector indicates the changes of  $R_h$  and precipitation per day computed by central differencing averaged in each bin. Bins containing less than 300 data points are discarded. The data are obtained from a horizontal grid of  $2.5^\circ \times 2.5^\circ$  in the area of  $10^\circ\text{S}$ – $10^\circ\text{N}$  and  $60^\circ$ – $180^\circ\text{E}$ .

and 22.0 hr for the observations, UNICON, and UNICON-STO, respectively. The reduced convective adjustment time scale in UNICON-STO indicates convection becomes more sensitive to environmental humidity. One factor that can explain the change in the convective adjustment time scale is the fractional entrainment rate of convection (Holloway & Neelin, 2009). SB23 demonstrated that the mean radius of updrafts is decreased due to the increased frequency of shallow cumulus in stochastic UNICON, which likely yields increases in the fractional entrainment rate and sensitivity to environmental humidity.

The vectors in the second row of Figure 10 show changes in  $R_h$  and  $P$  in a day. The trajectories along the vectors show the life cycles of tropical convective systems, showing clockwise evolution around an attractor (Wolding et al., 2020). Wolding et al. (2020) categorized precipitation types using the TRMM 2A23 data, where shallow convective precipitation occurs in low  $R_h$  and  $P$  regime, deep convective precipitation occurs in the moderately moist environment ( $0.6 < R_h < 0.8$ ) with high  $P$ , and stratiform precipitation occurs in the very moist environment ( $R_h > 0.8$ ). UNICON largely underestimates the magnitudes of daily tendencies of  $R_h$  and  $P$ , particularly for the positive tendencies in the deep convective precipitation regime (moderate  $R_h$ ). The weak positive  $R_h$  and  $P$  tendencies indicate a lack of driving mechanisms (e.g., moisture convergence) for developing organized convection. The positive  $R_h$  and  $P$  tendencies in the deep convective precipitation regime are considerably stronger in UNICON-STO, while they are still weaker than in the observation. The enhanced tendencies are also consistent with the increased frequency of intense precipitation. As will be discussed later, UNICON-STO exhibits stronger moistening tendencies in the MJO developing stage, which make a more favorable condition for developing organized convection.

The better simulation of daily tendencies of  $R_h$  and  $P$  in UNICON-STO implies enhanced feedback between shallow convection and low-level moisture convergence. The amplification or decay of day-to-day precipitation is controlled by the balance between horizontal moisture advection and the column process (e.g., Inoue et al., 2021). In a developing tropical convective system, it is known that shallow convection is important since the convective heating in the lower troposphere drives more moisture convergence than is removed by precipitation, resulting in a net moistening (Wolding & Maloney, 2015). The local effect of shallow convection alone is not able to

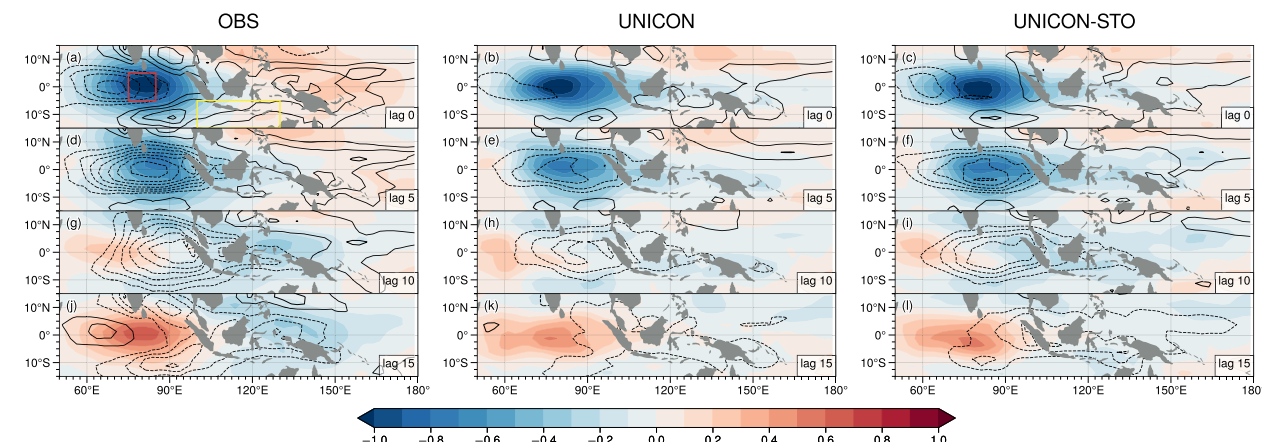


**Figure 11.** 20–100-day bandpass-filtered annual anomalies of outgoing longwave radiation (OLR) (shaded;  $\text{W m}^{-2}$ ) and precipitation tendency (contour;  $0.005 \text{ mm day}^{-2}$  intervals) regressed onto the OLR time series averaged in the area over the Indian Ocean ( $5^\circ\text{S}$ – $5^\circ\text{N}$ ,  $75^\circ$ – $85^\circ\text{E}$ ; the red box in (a)), obtained from (first column) the observations, (second column) UNICON, and (third column) UNICON-STO. The regression coefficients on lag 0, 5, 10, and 15 days are shown. The yellow box in (a) denotes the area over the southern Maritime Continent ( $15^\circ$ – $5^\circ\text{S}$ ,  $100^\circ$ – $140^\circ\text{E}$ ) where the precipitation budget terms are averaged in Figure S9 of Supporting Information S1.

sufficiently explain the moistening of the lower troposphere, so the modulation of large-scale circulation by shallow convection needs to be considered (Hohenegger & Stevens, 2013; Y. Liu et al., 2022). The following precipitation budget analysis will demonstrate that both horizontal moisture advection and the column process are enhanced in UNICON-STO.

Since the multivariate EOF modes of the observation and simulations are substantially different, compositing precipitation budget terms to a specific RMM phase does not provide a fair comparison between the observation and simulations. Therefore, we calculate lead-lag regressions of intraseasonal precipitation budget terms against area-averaged OLR time series in the area over the Indian Ocean ( $5^\circ\text{S}$ – $5^\circ\text{N}$ ,  $75^\circ$ – $85^\circ\text{E}$ ). We flip the sign of the regression coefficients for the figures so that the anomalies correspond to enhanced convection over the equatorial Indian Ocean. The value of the regression coefficient denotes a change in a variable against a decrease in  $1 \text{ W m}^{-2}$  of OLR. Figure 11 shows annual anomalies of OLR and precipitation tendencies on lag days 0–15 for the observation and simulations. The convection activity matures in the equatorial Indian Ocean on lag day 0, and the convection propagates across the Maritime Continent with increasing lag days. In the observation, positive precipitation tendencies (moisture recharging) precede about 10–15 days on the east of convection peaks, and negative precipitation tendencies follow the convection peaks on the west. The simulations show much weaker precipitation tendencies than the observation, and the simulated distributions of anomalies are somewhat different from the observation. The positive precipitation tendencies in the simulations propagate northeastward much faster and leave the Maritime Continent earlier than the observation. However, UNICON-STO simulates stronger precipitation tendencies and also better maintains negative OLR anomalies with longer lags compared to UNICON (note that negative OLR anomalies are stronger in lag day 10 over the Maritime Continent). Figures S7 and S8 in Supporting Information S1 are the same as Figure 11 but during summer and winter, respectively. The seasonal variations of precipitation tendencies and OLR anomalies are too large in the simulations. The anomalies are enhanced during both seasons in UNICON-STO compared to UNICON. The magnitudes of anomalies in UNICON-STO are similar to the observation during summer but are still underestimated during winter. Notably, during winter, UNICON fails to maintain moistening tendencies and negative OLR anomalies over the Maritime Continent region on lag day 15.

Figure 12 shows the horizontal distribution of individual precipitation budget terms on lag day 0. The sum of the four terms is approximately equal to the total precipitation tendencies (contour). The equality is not exact because of the numerical errors when computing budget terms. In the observation, the patterns of the zonal and meridional advection terms resemble that of the total precipitation tendency with the same polarity (Figures 12a and 12d), while the evaporation term shows the opposite polarity (Figure 12g). The convective column process enhances moisture tendency in the equatorial Indian Ocean and the Maritime Continent area (Figure 12j). The patterns of the precipitation budget terms are similarly reproduced in UNICON and UNICON-STO but with weaker amplitudes. There are some regions where UNICON does not simulate the contribution by the budget terms properly. For example, UNICON simulates

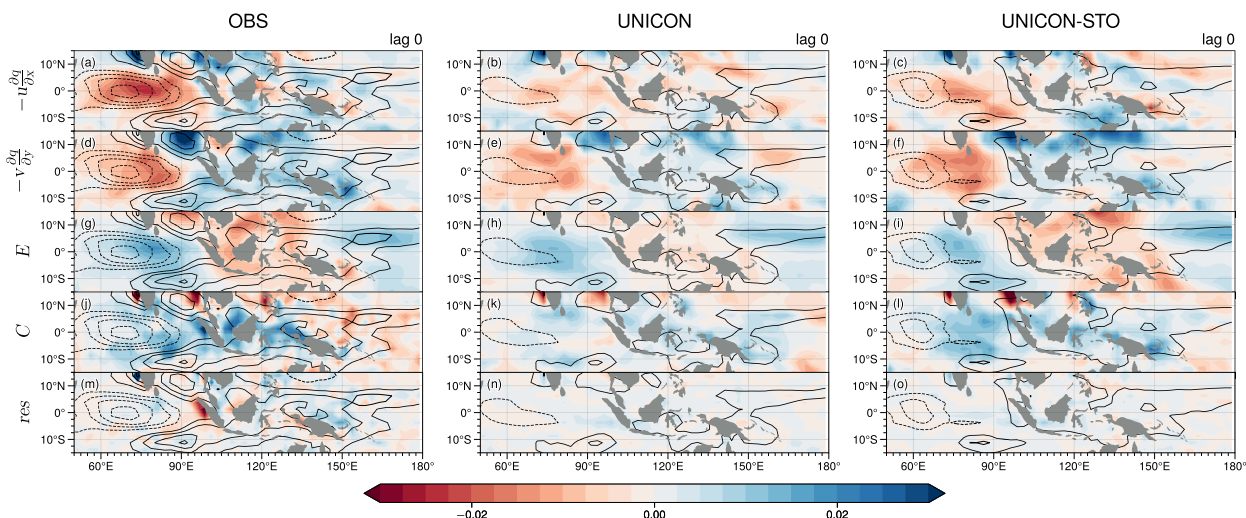


**Figure 12.** As in Figure 11, except that each precipitation budget term on lag day 0 is shaded. The budget residuals are denoted as *res*. The precipitation budget terms are in the unit of  $\text{mm day}^{-2}$ .

drying tendencies by zonal advection ( $-u\partial q/\partial x$ ) over the Maritime Continent area, while the observation shows moistening tendencies. In addition, UNICON simulates too weak moistening by convective column process over the eastern equatorial Indian Ocean and the Maritime Continent region. UNICON-STO alleviates these deficiencies and does a better job of reproducing magnitudes of tendencies by the budget terms. The analysis from Adames (2017) demonstrated that the moistening by the convective column process is associated with bottom-heavy baroclinic vertical motion (which is related to shallow convection), and the drying is associated with elevated stratiform convection. As mentioned above, bottom-heavy heating by shallow convection drives the large-scale upward motion and moisture convergence. In addition to this effect, shallow convection itself transports moisture from PBL to the lower free troposphere, leading to tropospheric moistening and increasing precipitation. The increased moistening tendencies by the convective column process in UNICON-STO are due to a better representation of shallow convection (see Figure S10 in Supporting Information S1 and its explanation). However, both UNICON and UNICON-STO do not reproduce drying tendencies by the convective column process over the western equatorial Pacific.

Figure 13 shows the regression coefficients of the precipitation budget terms averaged over the reference area over the Indian Ocean where the MJO events initiate. The first row of the figure shows averages during lag  $-15$  to lag  $0$  days (developing period), and the second row shows averages during lag  $0$  to lag  $15$  days (decaying period). During the developing period, mean moistening tendencies exist over the area, and the largest contribution comes from the convective column process, indicating that moistening from shallow convection is a critical factor. UNICON underestimates positive precipitation tendencies in the developing period largely due to the underestimation of the convective column process and zonal advection terms. Particularly, UNICON considerably underestimates the tendencies from the convective column process during winter, indicating that the initiation of winter MJO is suppressed in UNICON (Figure 13b). UNICON-STO displays larger total precipitation tendencies and the tendencies from zonal advection and convective column process during the developing period of all seasons, which are more consistent with the observation. Similarly, during the decaying period, UNICON underestimates total precipitation tendencies, and UNICON-STO simulates more realistic precipitation tendencies due to the increased contribution of horizontal advection terms. However, the convective column process terms in both simulations are underestimated in the decaying period, implying the unrealistic representation of stratiform precipitation systems in the simulations.

To investigate the propagation of the simulated winter MJO, the regression coefficients of budgets are averaged in the area over the southern Maritime Continent (Figure S9 in Supporting Information S1). Since the MJO detours southward of the Maritime Continent during boreal winter, the magnitudes of precipitation tendencies and budget terms during winter are much larger than those of summer. The largest contribution to the total tendencies comes from the horizontal advection terms, and a similar result is found in Kang et al. (2021). Consistent with the result above, UNICON-STO simulates improved precipitation tendencies and budget terms during early lag days in all seasons. Therefore, the improved winter MJO in UNICON-STO attributes to better simulation of moistening on the initiation of the MJO over the Indian Ocean and propagation over the southern Maritime Continent. The

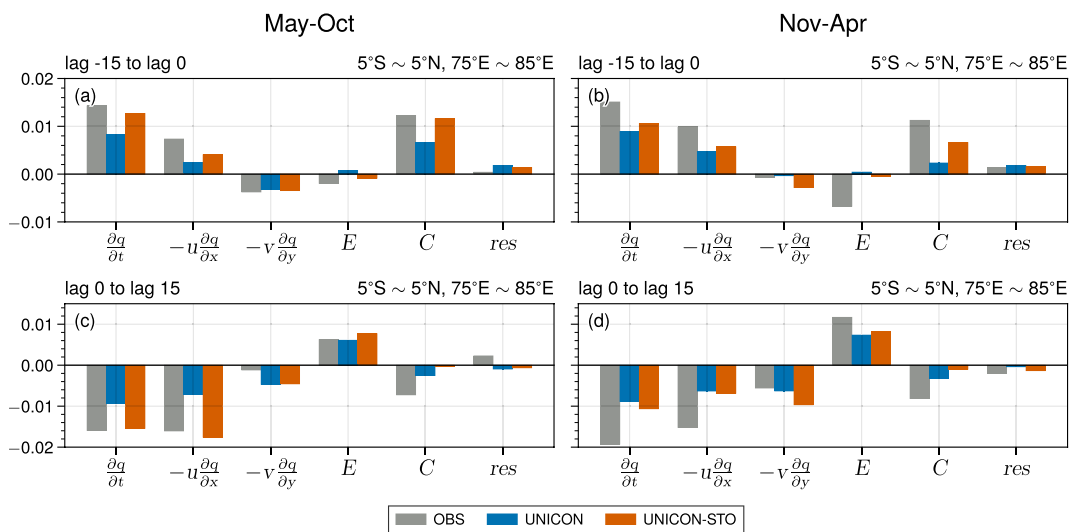


**Figure 13.** Regression coefficients of the precipitation budget terms averaged in the area over the Indian Ocean ( $5^{\circ}\text{S}$ – $5^{\circ}\text{N}$ ,  $75^{\circ}$ – $85^{\circ}\text{E}$ ; red box in Figure 11a). In (a and b), the regression coefficients are averaged during lag  $-15$  to lag  $0$  days for May–October and November–April, respectively. In (c and d), the regression coefficients are averaged during lag  $0$  to lag  $15$  days for May–October and November–April, respectively. The budget residuals are denoted as *res*.

improved horizontal moisture advection processes in UNICON-STO during winter are not likely due to the mean state change because the horizontal gradient of moisture is decreased (Figure 4).

Lastly, the vertical structures of the simulated MJO are investigated. The vertical-longitudinal profiles of regression coefficients of several atmospheric variables are plotted (Figure 14). Jiang et al. (2015) showed that the CMIP5 models with good MJO simulations reproduce vertically tilted structures of anomalous  $T$ ,  $q$ , and  $\omega$  in observations, so the vertical structure of intraseasonal anomalies can be used as a measure of model performance on convective processes. The convection peak at  $75^{\circ}$ – $85^{\circ}\text{E}$  is associated with anomalous horizontal wind convergence (Figure 14a) and large-scale ascent motion (Figure 14b). The top-heavy temperature anomalies come from the strong diabatic heating at the main convection region (Jiang et al., 2015). The temperature anomalies show westward vertical tilts due to the lowering of convection height in the eastward direction (Figure 14c). The simulations reproduce the observed vertical MJO structure reasonably well but with some discrepancies in the detailed structure. For instance, both UNICON and UNICON-STO show excessive cooling in the lower troposphere during the developing and mature stages of the MJO active phase. Compared to UNICON, UNICON-STO simulates more pronounced positive specific humidity and moist static energy anomalies below 700 hPa at the east of the main convection region, signaling a better representation of the preconditioning process for the eastward propagation of the MJO. The anomalies are also enhanced in the main convection region in UNICON-STO, implying that the increased moistening intensified organized convection.

Figure S10 shows vertical profiles of regression coefficients of vertical pressure velocity as a function of lag days. During the MJO developing (decaying) stage, the observed large-scale vertical velocity is bottom-heavy (top-heavy). UNICON-STO reduces positive pressure velocity biases of UNICON during the developing stage, especially in the lower troposphere, implying that convection is more bottom-heavy in UNICON-STO. Both simulations have vertical velocity profiles of being too bottom-heavy during the decaying stage, and the result reveals why the column processes of the simulations are underestimated during the decaying stage. This might indicate the deficiency of the convection scheme where stratiform precipitation systems in the MJO decaying stage (anvil clouds) are not realistically simulated, as shown in SB23.

#### 4. Summary and Conclusions

In this study, we evaluate the global climate simulation with a stochastic unified convection scheme (stochastic UNICON; UNICON-STO in short), focusing on the simulation of the MJO. Stochastic UNICON randomly initializes convective updrafts from a joint PDF of thermodynamic variables and updraft radius at the near-surface. Stochastic UNICON extends the original UNICON, which is a bulk plume model, to a spectral plume model,

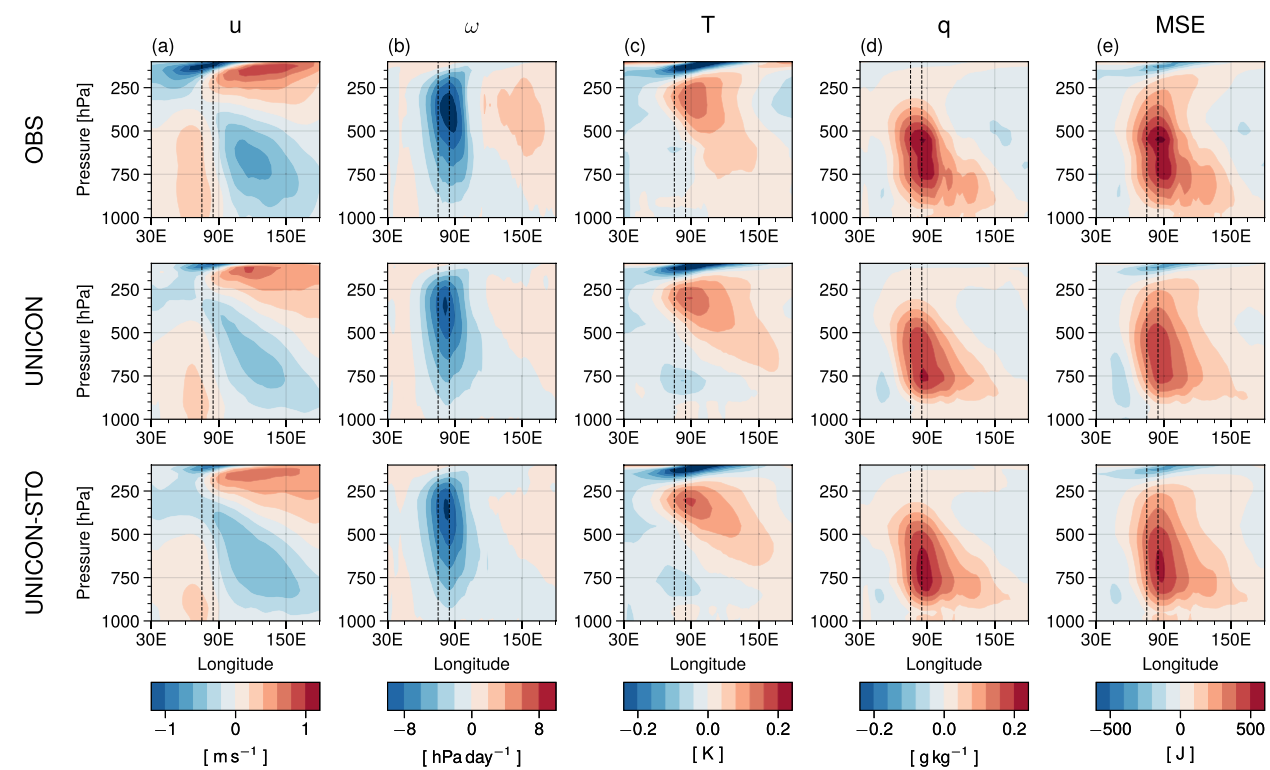


**Figure 14.** Vertical-longitudinal profiles of annual zero lag-regression coefficients of the intraseasonal anomalies of zonal wind ( $u$ ), vertical pressure velocity ( $\omega$ ), temperature ( $T$ ), specific humidity ( $q$ ), and moist static energy averaged over the latitude band of  $10^{\circ}\text{S}$ – $10^{\circ}\text{N}$ . The vertical dashed lines denote the latitudes of the reference area over the Indian Ocean.

where the scheme produces a spectrum of convective updrafts in a physically based manner. Two AMIP simulations using the SAM0-UNICON atmospheric GCM with UNICON and stochastic UNICON are conducted for the period 1979–2014 and compared with observations.

The model performances on reproducing observed mean state are evaluated using a Taylor diagram of 10 climate variables. The mean RMSEs in UNICON and UNICON-STO are almost identical, while the mean bias is reduced by 18% from UNICON to UNICON-STO. The reduction of the mean bias largely comes from the alleviation of the mean negative shortwave cloud forcing (SWCF) bias presented in UNICON, and the result is consistent with the reduction of low cloud fraction. UNICON-STO simulates much more frequent shallow convection, and the increased shallow convective heating. In this regard, positive relative humidity biases over mid-high latitudes presented in UNICON are slightly reduced and mean SWCF is increased in UNICON-STO. Nevertheless, the general performance of UNICON-STO is comparable to UNICON and does not show systematic improvements in mean states. For instance, the spatial-temporal correlation of relative humidity is increased, but that of land precipitation is decreased in UNICON-STO.

Next, we evaluate the simulations on reproducing observed MJO characteristics using various MJO diagnostics. Although SAM0-UNICON is one of the CMIP6 models that have relatively good MJO simulation performance (Le et al., 2021), UNICON-STO further improves various properties of the MJO. A spectrum analysis indicates that UNICON-STO better reproduces the wave power maximum in the intraseasonal time scale, while UNICON produces the power maximum at a lower frequency regime. Particularly, UNICON-STO substantially improves the power of winter MJO, while UNICON simulates too weak winter MJO. UNICON-STO also enhances the wave coherency between OLR and 850 hPa zonal wind for the wave components related to the MJO, which UNICON underestimates. The lead-lag correlation analysis indicates that UNICON substantially underestimates the strengths of eastward propagation of convection and associated wind anomalies during winter, and UNICON-STO simulates more realistic propagation patterns. UNICON-STO also improves the magnitudes and horizontal distributions of anomalies associated with the MJO life cycle, especially when convection is active over the

Maritime Continent or western equatorial Pacific. Still, both simulations have a common problem that simulated intraseasonal variabilities are too strong over the central and eastern equatorial Pacific.

The relationship between moisture and precipitation is closely related to the life cycles of tropical convective systems and MJO. The relationship between CRH ( $R_h$ ) and precipitation ( $P$ ) is hypothesized as an exponential function of  $P = P_0 \exp(aR_h)$ . The fitted values of  $a$  in the observation, UNICON, and UNICON-STO are 13.95, 9.62, and 11.55, respectively. UNICON-STO has a larger value of  $a$  (and smaller convective adjustment time scale) than UNICON because UNICON-STO produces more frequent intense precipitation over the tropics, which better matches with the TRMM observation. These results indicate stronger development of organized convection and increased sensitivity of convection to environmental humidity, in UNICON-STO. It is found that UNICON-STO displays stronger positive  $R_h$  and  $P$  tendencies in the deep convective precipitation regime, implying that stronger moisture convergence is induced by shallow convection.

To decompose the processes that induce moisture tendencies, the precipitation budget analysis is conducted. The magnitudes of intraseasonal moisture (precipitation) tendencies are underestimated in both simulations, but UNICON-STO shows larger total tendencies and budget terms compared to UNICON. UNICON-STO better reproduces moistening tendencies by zonal advection over the Maritime Continent area and by convective column process over the eastern equatorial Indian Ocean. During the MJO development stage over the Indian Ocean, UNICON-STO simulates increased moistening tendencies primarily due to the enhanced convective column process. The vertical structures of MJO-related anomalies confirm that these moistening tendencies are located in the lower troposphere before convection matures. We also demonstrate that the moistening tendency by advection over the southern Maritime Continent is enhanced during winter in UNICON-STO, which explains better simulation of the winter MJO.

From the precipitation budget analysis, the enhancements of MJO amplitude and propagation in UNICON-STO are related to the change in the relationship between moisture and convection. The enhancement is less likely to be related to the mean state change because the lower-tropospheric moisture biases are not mitigated from UNICON to UNION-STO. While the budget explains the enhancement to some extent, what is not revealed in this study is why the MJO enhancement is more evident in winter than in summer. We need to examine other mechanisms that affect the characteristics of simulated MJO to understand the seasonal difference better. The diurnal cycle over the Maritime Continent and the convection-radiation interaction are important factors that need to be investigated.

This study emphasizes the importance of the representation of shallow convection in a GCM for realistic MJO simulation. The spectral representation of convection in a GCM is one way of improving the representation of shallow convection. Such a model can help understand how convective clouds with different scales interact. We can investigate intraseasonal variabilities of physical tendencies, mass fluxes, and fractional entrainment rates for different types of convection. However, it requires a model to output a large number of four-dimensional variables in high frequency, so we will leave this subject as a future study. In addition, MJO simulations in a fully-coupled model and with different model resolutions are important issues that need to be investigated.

## Data Availability Statement

The global simulation outputs (climatologies and daily anomalies), calculated RMM indexes, and the results of the budget analysis are available at <https://doi.org/10.5281/zenodo.7412470> (Shin & Baik, 2022). The daily Tropical Rainfall Measuring Mission 3B42 version 7 (TRMM 3B42v7) data can be obtained from the website ([https://disc.gsfc.nasa.gov/datasets/TRMM\\_3B42\\_Daily\\_7/summary](https://disc.gsfc.nasa.gov/datasets/TRMM_3B42_Daily_7/summary); G. J. Huffman et al., 2016). The fifth generation of the ECMWF reanalysis (ERA5) data can be obtained from the website (<https://cds.climate.copernicus.eu/cdsapp#!/home>; Copernicus Climate Change Service (C3S), 2017).

## References

- Adames, Á. F. (2017). Precipitation budget of the Madden-Julian oscillation. *Journal of the Atmospheric Sciences*, 74(6), 1799–1817. <https://doi.org/10.1175/jas-d-16-0242.1>
- Adames, Á. F., Wallace, J. M., & Monteiro, J. M. (2016). Seasonality of the structure and propagation characteristics of the MJO. *Journal of the Atmospheric Sciences*, 73(9), 3511–3526. <https://doi.org/10.1175/jas-d-15-0232.1>
- Adler, R. F., Huffman, G. J., Chang, A., Ferraro, R., Xie, P.-P., Janowiak, J., et al. (2003). The version-2 global precipitation climatology project (GPCP) monthly precipitation analysis (1979–present). *Journal of Hydrometeorology*, 4(6), 1147–1167. [https://doi.org/10.1175/1525-7541\(2003\)004<1147:tvgpc>2.0.co;2](https://doi.org/10.1175/1525-7541(2003)004<1147:tvgpc>2.0.co;2)

## Acknowledgments

The authors are grateful to three anonymous reviewers for providing valuable comments on this work. This work was supported by the National Research Foundation of Korea (NRF) grant funded by the Korea government (MSIT) (No. RS-2023-00214037). This work was also supported by the National Research Foundation of Korea (NRF) under Grant 2021R1A2C1007044 and supported by the National Supercomputing Center with supercomputing resources including technical support (KSC-2021-CRE-0475).

- Ahn, M.-S., Kim, D., Kang, D., Lee, J., Sperber, K. R., Gleckler, P. J., et al. (2020). MJO propagation across the Maritime Continent: Are CMIP6 models better than CMIP5 models? *Geophysical Research Letters*, 47(11), e2020GL087250. <https://doi.org/10.1029/2020gl087250>
- Ahn, M.-S., Kim, D., Park, S., & Ham, Y.-G. (2019). Do we need to parameterize mesoscale convective organization to mitigate the MJO-mean state trade-off? *Geophysical Research Letters*, 46(4), 2293–2301. <https://doi.org/10.1029/2018gl080314>
- Ahn, M.-S., Kim, D., Sperber, K. R., Kang, I.-S., Maloney, E., Waliser, D., & Hendon, H. (2017). MJO simulation in CMIP5 climate models: MJO skill metrics and process-oriented diagnosis. *Climate Dynamics*, 49(11), 4023–4045. <https://doi.org/10.1007/s00382-017-3558-4>
- Baba, Y. (2019). Spectral cumulus parameterization based on cloud-resolving model. *Climate Dynamics*, 52(1), 309–334. <https://doi.org/10.1007/s00382-018-4137-z>
- Baba, Y. (2021). Improved intraseasonal variability in the initialization of SINTEX-F2 using a spectral cumulus parameterization. *International Journal of Climatology*, 41(15), 6690–6712. <https://doi.org/10.1002/joc.7220>
- Baba, Y., & Giorgetta, M. A. (2020). Tropical variability simulated in ICON-A with a spectral cumulus parameterization. *Journal of Advances in Modeling Earth Systems*, 12(1), e2019MS001732. <https://doi.org/10.1029/2019ms001732>
- Benedict, J. J., & Randall, D. A. (2007). Observed characteristics of the MJO relative to maximum rainfall. *Journal of the Atmospheric Sciences*, 64(7), 2332–2354. <https://doi.org/10.1175/jas3968.1>
- Bentamy, A., Queffeulou, P., Quilfen, Y., & Katsaros, K. (1999). Ocean surface wind fields estimated from satellite active and passive microwave instruments. *IEEE Transactions on Geoscience and Remote Sensing*, 37(5), 2469–2486. <https://doi.org/10.1109/36.789643>
- Betts, A., & Miller, M. (1986). A new convective adjustment scheme. Part II: Single column tests using GATE wave, BOMEX, ATEX and arctic air-mass data sets. *Quarterly Journal of the Royal Meteorological Society*, 112(473), 693–709. <https://doi.org/10.1002/qj.49711247308>
- Bretherton, C. S., & Park, S. (2009). A new moist turbulence parameterization in the community atmosphere model. *Journal of Climate*, 22(12), 3422–3448. <https://doi.org/10.1175/2008jcli2556.1>
- Bretherton, C. S., Peters, M. E., & Back, L. E. (2004). Relationships between water vapor path and precipitation over the tropical oceans. *Journal of Climate*, 17(7), 1517–1528. [https://doi.org/10.1175/1520-0442\(2004\)017<1517:rbwvpa>2.0.co;2](https://doi.org/10.1175/1520-0442(2004)017<1517:rbwvpa>2.0.co;2)
- Cai, Q., Zhang, G. J., & Zhou, T. (2013). Impacts of shallow convection on MJO simulation: A moist static energy and moisture budget analysis. *Journal of Climate*, 26(8), 2417–2431. <https://doi.org/10.1175/jcli-d-12-00127.1>
- Camargo, S. J., Wheeler, M. C., & Sobel, A. H. (2009). Diagnosis of the MJO modulation of tropical cyclogenesis using an empirical index. *Journal of the Atmospheric Sciences*, 66(10), 3061–3074. <https://doi.org/10.1175/2009jas3101.1>
- Chen, B., & Mapes, B. E. (2018). Effects of a simple convective organization scheme in a two-plume GCM. *Journal of Advances in Modeling Earth Systems*, 10(3), 867–880. <https://doi.org/10.1002/2017ms001106>
- Chen, C.-C., Richter, J. H., Liu, C., Moncrieff, M. W., Tang, Q., Lin, W., et al. (2021). Effects of organized convection parameterization on the MJO and precipitation in E3SMv1. Part I: Mesoscale heating. *Journal of Advances in Modeling Earth Systems*, 13(6), e2020MS002401. <https://doi.org/10.1029/2020ms002401>
- Chen, G., Ling, J., Zhang, R., Xiao, Z., & Li, C. (2022). The MJO from CMIP5 to CMIP6: Perspectives from tracking MJO precipitation. *Geophysical Research Letters*, 49(1), e2021GL095241. <https://doi.org/10.1029/2021gl095241>
- Chen, S. S., Houze, R. A., & Mapes, B. E. (1996). Multiscale variability of deep convection in relation to large-scale circulation in TOGA COARE. *Journal of the Atmospheric Sciences*, 53(10), 1380–1409. [https://doi.org/10.1175/1520-0469\(1996\)053<1380:mvodci>2.0.co;2](https://doi.org/10.1175/1520-0469(1996)053<1380:mvodci>2.0.co;2)
- Copernicus Climate Change Service (C3S). (2017). ERA5: Fifth generation of ECMWF atmospheric reanalyses of the global climate [Dataset]. Copernicus Climate Change Service Climate Data Store (CDS). Retrieved from <https://cds.climate.copernicus.eu/cdsapp#!/>
- Derbyshire, S. H., Beau, I., Bechtold, P., Grandpeix, J.-Y., Piriou, J.-M., Redelsperger, J.-L., & Soares, P. M. M. (2004). Sensitivity of moist convection to environmental humidity. *Quarterly Journal of the Royal Meteorological Society*, 130(604), 3055–3079. <https://doi.org/10.1256/qj.03.130>
- Eyring, V., Bony, S., Meehl, G. A., Senior, C. A., Stevens, B., Stouffer, R. J., & Taylor, K. E. (2016). Overview of the Coupled Model Inter-comparison Project Phase 6 (CMIP6) experimental design and organization. *Geoscientific Model Development*, 9(5), 1937–1958. <https://doi.org/10.5194/gmd-9-1937-2016>
- Frierson, D. M. W. (2007). The dynamics of idealized convection schemes and their effect on the zonally averaged tropical circulation. *Journal of the Atmospheric Sciences*, 64(6), 1959–1976. <https://doi.org/10.1175/jas3935.1>
- Gonzalez, A. O., & Jiang, X. (2017). Winter mean lower tropospheric moisture over the Maritime Continent as a climate model diagnostic metric for the propagation of the Madden-Julian oscillation. *Geophysical Research Letters*, 44(5), 2588–2596. <https://doi.org/10.1002/2016gl072430>
- Hall, J. D., Matthews, A. J., & Karoly, D. J. (2001). The modulation of tropical cyclone activity in the Australian region by the Madden-Julian oscillation. *Monthly Weather Review*, 129(12), 2970–2982. [https://doi.org/10.1175/1520-0493\(2001\)129<2970:tmotca>2.0.co;2](https://doi.org/10.1175/1520-0493(2001)129<2970:tmotca>2.0.co;2)
- Hannah, W. M., & Maloney, E. D. (2011). The role of moisture–convection feedbacks in simulating the Madden-Julian oscillation. *Journal of Climate*, 24(11), 2754–2770. <https://doi.org/10.1175/2011jcli3803.1>
- Hendon, H. H., Wheeler, M. C., & Zhang, C. (2007). Seasonal dependence of the MJO–ENSO relationship. *Journal of Climate*, 20(3), 531–543. <https://doi.org/10.1175/jcli4003.1>
- Hersbach, H., Bell, B., Berrisford, P., Hirahara, S., Horányi, A., Muñoz-Sabater, J., et al. (2020). The ERA5 global reanalysis. *Quarterly Journal of the Royal Meteorological Society*, 146(730), 1999–2049. <https://doi.org/10.1002/qj.3803>
- Heus, T., & Seifert, A. (2013). Automated tracking of shallow cumulus clouds in large domain, long duration large eddy simulations. *Geoscientific Model Development*, 6(4), 1261–1273. <https://doi.org/10.5194/gmd-6-1261-2013>
- Hohenegger, C., & Stevens, B. (2013). Preconditioning deep convection with cumulus congestus. *Journal of the Atmospheric Sciences*, 70(2), 448–464. <https://doi.org/10.1175/jas-d-12-089.1>
- Holloway, C., & Neelin, J. (2009). Moisture vertical structure, column water vapor, and tropical deep convection. *Journal of the Atmospheric Sciences*, 66(6), 1665–1683. <https://doi.org/10.1175/2008jas2806.1>
- Hsu, H.-H., & Lee, M.-Y. (2005). Topographic effects on the eastward propagation and initiation of the Madden–Julian oscillation. *Journal of Climate*, 18(6), 795–809. <https://doi.org/10.1175/jcli-3292.1>
- Huffman, G. J., Bolvin, D. T., Nelkin, E. J., & Adler, R. F. (2016). TRMM (TMPA) Precipitation L3 1 day 0.25 degree x 0.25 degree V7 [Dataset]. Goddard Earth Sciences Data and Information Services Center (GES DISC). <https://doi.org/10.5067/TRMM/TMPA/DAY7>
- Huffman, G. J., Bolvin, D. T., Nelkin, E. J., Wolff, D. B., Adler, R. F., Gu, G., et al. (2007). The TRMM Multisatellite Precipitation Analysis (TMPA): Quasi-global, multiyear, combined-sensor precipitation estimates at fine scales. *Journal of Hydrometeorology*, 8(1), 38–55. <https://doi.org/10.1175/jhm560.1>
- Iacono, M. J., Delamere, J. S., Mlawer, E. J., Shephard, M. W., Clough, S. A., & Collins, W. D. (2008). Radiative forcing by long-lived greenhouse gases: Calculations with the AER radiative transfer models. *Journal of Geophysical Research*, 113(D13), D13103. <https://doi.org/10.1029/2008jd009944>

- Inoue, K., Biasutti, M., & Fridlind, A. M. (2021). Evidence that horizontal moisture advection regulates the ubiquitous amplification of rainfall variability over tropical oceans. *Journal of the Atmospheric Sciences*, 78(2), 529–547. <https://doi.org/10.1175/jas-d-20-0201.1>
- Janiga, M. A., & Zhang, C. (2016). MJO moisture budget during DYNAMO in a cloud-resolving model. *Journal of the Atmospheric Sciences*, 73(6), 2257–2278. <https://doi.org/10.1175/jas-d-14-0379.1>
- Jiang, X. (2017). Key processes for the eastward propagation of the Madden-Julian Oscillation based on multimodel simulations. *Journal of Geophysical Research: Atmospheres*, 122(2), 755–770. <https://doi.org/10.1002/2016jd025955>
- Jiang, X., Waliser, D. E., Xavier, P. K., Petch, J., Klingaman, N. P., Woolnough, S. J., et al. (2015). Vertical structure and physical processes of the Madden-Julian oscillation: Exploring key model physics in climate simulations. *Journal of Geophysical Research: Atmospheres*, 120(10), 4718–4748. <https://doi.org/10.1002/2014jd022375>
- Kang, D., Kim, D., Ahn, M.-S., & An, S.-I. (2021). The role of the background meridional moisture gradient on the propagation of the MJO over the Maritime Continent. *Journal of Climate*, 34(16), 6565–6581.
- Kang, D., Kim, D., Ahn, M.-S., Neale, R., Lee, J., & Gleckler, P. J. (2020). The role of the mean state on MJO simulation in CESM2 ensemble simulation. *Geophysical Research Letters*, 47(24), e2020GL089824. <https://doi.org/10.1029/2020gl089824>
- Kim, D., Kim, H., & Lee, M.-I. (2017). Why does the MJO detour the Maritime Continent during austral summer? *Geophysical Research Letters*, 44(5), 2579–2587. <https://doi.org/10.1002/2017gl072643>
- Kim, D., Sobel, A. H., Maloney, E. D., Frierson, D. M., & Kang, I.-S. (2011). A systematic relationship between intraseasonal variability and mean state bias in AGCM simulations. *Journal of Climate*, 24(21), 5506–5520. <https://doi.org/10.1175/2011jcli4177.1>
- Lavender, S. L., & Matthews, A. J. (2009). Response of the West African monsoon to the Madden-Julian oscillation. *Journal of Climate*, 22(15), 4097–4116. <https://doi.org/10.1175/2009jcli2773.1>
- Le, P. V., Guillotau, C., Mamalakis, A., & Foufoula-Georgiou, E. (2021). Underestimated MJO variability in CMIP6 models. *Geophysical Research Letters*, 48(12), e2020GL092244. <https://doi.org/10.1029/2020gl092244>
- Lee, R. W., Woolnough, S. J., Charlton-Perez, A. J., & Vitart, F. (2019). ENSO modulation of MJO teleconnections to the North Atlantic and Europe. *Geophysical Research Letters*, 46(22), 13535–13545. <https://doi.org/10.1029/2019gl084683>
- Liebmann, B., Hendon, H. H., & Glick, J. D. (1994). The relationship between tropical cyclones of the western Pacific and Indian Oceans and the Madden-Julian oscillation. *Journal of the Meteorological Society of Japan. Ser. II*, 72(3), 401–412. [https://doi.org/10.2151/jmsj1965.72.3\\_401](https://doi.org/10.2151/jmsj1965.72.3_401)
- Liebmann, B., & Smith, C. A. (1996). Description of a complete (interpolated) outgoing longwave radiation dataset. *Bulletin of the American Meteorological Society*, 77(6), 1275–1277.
- Lin, S.-J., & Rood, R. B. (1996). Multidimensional flux-form semi-Lagrangian transport schemes. *Monthly Weather Review*, 124(9), 2046–2070. [https://doi.org/10.1175/1520-0493\(1996\)124<2046:mfsl>2.0.co;2](https://doi.org/10.1175/1520-0493(1996)124<2046:mfsl>2.0.co;2)
- Liu, X., Easter, R. C., Ghan, S. J., Zaveri, R., Rasch, P., Shi, X., et al. (2012). Toward a minimal representation of aerosols in climate models: Description and evaluation in the Community Atmosphere Model CAM5. *Geoscientific Model Development*, 5(3), 709–739. <https://doi.org/10.5194/gmd-5-709-2012>
- Liu, Y., Tan, Z.-M., & Wu, Z. (2022). Enhanced feedback between shallow convection and low-level moisture convergence leads to improved simulation of MJO eastward propagation. *Journal of Climate*, 35(2), 591–615. <https://doi.org/10.1175/jcli-d-20-0894.1>
- Loeb, N. G., Wielicki, B. A., Doelling, D. R., Smith, G. L., Keyes, D. F., Kato, S., et al. (2009). Toward optimal closure of the earth's top-of-atmosphere radiation budget. *Journal of Climate*, 22(3), 748–766. <https://doi.org/10.1175/2008jcli2637.1>
- Lorenz, D. J., & Hartmann, D. L. (2006). The effect of the MJO on the North American monsoon. *Journal of Climate*, 19(3), 333–343. <https://doi.org/10.1175/jcli3684.1>
- Madden, R. A., & Julian, P. R. (1971). Detection of a 40–50 day oscillation in the zonal wind in the tropical Pacific. *Journal of the Atmospheric Sciences*, 28(5), 702–708. [https://doi.org/10.1175/1520-0469\(1971\)028<0702:doadoi>2.0.co;2](https://doi.org/10.1175/1520-0469(1971)028<0702:doadoi>2.0.co;2)
- Maloney, E. D., & Hartmann, D. L. (2000a). Modulation of eastern North Pacific hurricanes by the Madden-Julian oscillation. *Journal of Climate*, 13(9), 1451–1460. [https://doi.org/10.1175/1520-0442\(2000\)013<1451:moenph>2.0.co;2](https://doi.org/10.1175/1520-0442(2000)013<1451:moenph>2.0.co;2)
- Maloney, E. D., & Hartmann, D. L. (2000b). Modulation of hurricane activity in the Gulf of Mexico by the Madden-Julian oscillation. *Science*, 287(5460), 2002–2004. <https://doi.org/10.1126/science.287.5460.2002>
- Moon, J.-Y., Wang, B., & Ha, K.-J. (2011). ENSO regulation of MJO teleconnection. *Climate Dynamics*, 37(5), 1133–1149. <https://doi.org/10.1007/s00382-010-0902-3>
- Morrison, H., & Gettelman, A. (2008). A new two-moment bulk stratiform cloud microphysics scheme in the Community Atmosphere Model, version 3 (CAM3). Part I: Description and numerical tests. *Journal of Climate*, 21(15), 3642–3659. <https://doi.org/10.1175/2008jcli2105.1>
- Neale, R., & Slingo, J. (2003). The Maritime Continent and its role in the global climate: A GCM study. *Journal of Climate*, 16(5), 834–848. [https://doi.org/10.1175/1520-0442\(2003\)016<0834:tmcair>2.0.co;2](https://doi.org/10.1175/1520-0442(2003)016<0834:tmcair>2.0.co;2)
- Neggers, R. (2015). Exploring bin-macrophysics models for moist convective transport and clouds. *Journal of Advances in Modeling Earth Systems*, 7(4), 2079–2104. <https://doi.org/10.1002/2015ms000502>
- Neggers, R., Griewank, P., & Heus, T. (2019). Power-law scaling in the internal variability of cumulus cloud size distributions due to subsampling and spatial organization. *Journal of the Atmospheric Sciences*, 76(6), 1489–1503. <https://doi.org/10.1175/jas-d-18-0194.1>
- Neggers, R., Jonker, H., & Siebesma, A. (2003). Size statistics of cumulus cloud populations in large-eddy simulations. *Journal of the Atmospheric Sciences*, 60(8), 1060–1074. [https://doi.org/10.1175/1520-0469\(2003\)60<1060:scoccp>2.0.co;2](https://doi.org/10.1175/1520-0469(2003)60<1060:scoccp>2.0.co;2)
- O'Brien, T. A., Li, F., Collins, W. D., Rauscher, S. A., Ringler, T. D., Taylor, M., et al. (2013). Observed scaling in clouds and precipitation and scale incognizance in regional to global atmospheric models. *Journal of Climate*, 26(23), 9313–9333. <https://doi.org/10.1175/jcli-d-13-00005.1>
- Orbe, C., Roekel, L. V., Adames, Á. F., Dezfuli, A., Fasullo, J., Gleckler, P. J., et al. (2020). Representation of modes of variability in six US climate models. *Journal of Climate*, 33(17), 7591–7617. <https://doi.org/10.1175/jcli-d-19-0956.1>
- Park, S. (2014). A unified convection scheme (UNICON). Part I: Formulation. *Journal of the Atmospheric Sciences*, 71(11), 3902–3930. <https://doi.org/10.1175/jas-d-13-0233.1>
- Park, S., Baek, E.-H., Kim, B.-M., & Kim, S.-J. (2017). Impact of detrained cumulus on climate simulated by the Community Atmosphere Model Version 5 with a unified convection scheme. *Journal of Advances in Modeling Earth Systems*, 9(2), 1399–1411. <https://doi.org/10.1002/2016ms000877>
- Park, S., Bretherton, C. S., & Rasch, P. J. (2014). Integrating cloud processes in the community atmosphere model, version 5. *Journal of Climate*, 27(18), 6821–6856. <https://doi.org/10.1175/jcli-d-14-00087.1>
- Park, S., Shin, J., Kim, S., Oh, E., & Kim, Y. (2019). Global climate simulated by the Seoul National University atmosphere model version 0 with a unified convection scheme (SAM0-UNICON). *Journal of Climate*, 32(10), 2917–2949. <https://doi.org/10.1175/jcli-d-18-0796.1>
- Pincus, R., Barker, H. W., & Morette, J.-I. (2003). A fast, flexible, approximate technique for computing radiative transfer in inhomogeneous cloud fields. *Journal of Geophysical Research*, 108(D13), 4376. <https://doi.org/10.1029/2002jd003322>

- Powell, S. W., & Houze, R. A., Jr. (2013). The cloud population and onset of the Madden-Julian oscillation over the Indian Ocean during DYNAMO-AMIE. *Journal of Geophysical Research: Atmospheres*, 118(21), 11979–11995. <https://doi.org/10.1002/2013jd020421>
- Rushley, S. S., Kim, D., Bretherton, C. S., & Ahn, M.-S. (2018). Reexamining the nonlinear moisture-precipitation relationship over the tropical oceans. *Geophysical Research Letters*, 45(2), 1133–1140. <https://doi.org/10.1002/2017gl076296>
- Schiemann, R., Demory, M.-E., Mizielinski, M. S., Roberts, M. J., Shaffrey, L. C., Strachan, J., & Vidale, P. L. (2014). The sensitivity of the tropical circulation and Maritime Continent precipitation to climate model resolution. *Climate Dynamics*, 42(9), 2455–2468. <https://doi.org/10.1007/s00382-013-1997-0>
- Shin, J., & Baik, J.-J. (2022). Dataset for “Global Simulation of the Madden-Julian Oscillation With Stochastic Unified Convection Scheme” [Dataset]. Zenodo <https://doi.org/10.5281/zenodo.7412470>
- Shin, J., & Baik, J.-J. (2023). Optimization and evaluation of stochastic unified convection using single-column model simulations at multiple observation sites. *Journal of Advances in Modeling Earth Systems*, 15(5), e2022MS003473. <https://doi.org/10.1029/2022ms003473>
- Shin, J., & Park, S. (2020a). Impacts of ENSO and Madden-Julian oscillation on the genesis of tropical cyclones simulated by general circulation models and compared to observations. *Environmental Research Letters*, 15(3), 034046. <https://doi.org/10.1088/1748-9326/ab7466>
- Shin, J., & Park, S. (2020b). A stochastic unified convection scheme (UNICON). Part I: Formulation and single-column simulation for shallow convection. *Journal of the Atmospheric Sciences*, 77(2), 583–610. <https://doi.org/10.1175/jas-d-19-0117.1>
- Simmons, A., Uppala, S., Dee, D., & Kobayashi, S. (2007). ERA-Interim: New ECMWF reanalysis products from 1989 onwards. *ECMWF Newsletter*, 110(110), 25–35.
- Singh, S. V., Kripalani, R. H., & Sikka, D. R. (1992). Interannual variability of the Madden-Julian oscillations in Indian summer monsoon rainfall. *Journal of Climate*, 5(9), 973–978. [https://doi.org/10.1175/1520-0442\(1992\)005<0973:ivotmj>2.0.co;2](https://doi.org/10.1175/1520-0442(1992)005<0973:ivotmj>2.0.co;2)
- Suselj, K., Kurowski, M. J., & Teixeira, J. (2019). A unified eddy-diffusivity/mass-flux approach for modeling atmospheric convection. *Journal of the Atmospheric Sciences*, 76(8), 2505–2537. <https://doi.org/10.1175/jas-d-18-0239.1>
- Taraphdar, S., Zhang, F., Leung, L. R., Chen, X., & Pauluis, O. M. (2018). MJO affects the monsoon onset timing over the Indian region. *Geophysical Research Letters*, 45(18), 10011–10018. <https://doi.org/10.1029/2018gl078804>
- Taylor, K. E. (2001). Summarizing multiple aspects of model performance in a single diagram. *Journal of Geophysical Research*, 106(D7), 7183–7192. <https://doi.org/10.1029/2000jd900719>
- Waliser, D., Sperber, K., Hendon, H., Kim, D., Maloney, E., Wheeler, M., et al. (2009). MJO simulation diagnostics. *Journal of Climate*, 22(11), 3006–3030.
- Wheeler, M. C., & Hendon, H. H. (2004). An all-season real-time multivariate MJO index: Development of an index for monitoring and prediction. *Monthly Weather Review*, 132(8), 1917–1932. [https://doi.org/10.1175/1520-0493\(2004\)132<1917:armmi>2.0.co;2](https://doi.org/10.1175/1520-0493(2004)132<1917:armmi>2.0.co;2)
- Willmott, C. J., & Matsuura, K. (1995). Smart interpolation of annually averaged air temperature in the United States. *Journal of Applied Meteorology*, 34(12), 2577–2586. [https://doi.org/10.1175/1520-0450\(1995\)034<2577:siaaa>2.0.co;2](https://doi.org/10.1175/1520-0450(1995)034<2577:siaaa>2.0.co;2)
- Wolding, B. O., Dias, J., Kiladis, G., Ahmed, F., Powell, S. W., Maloney, E., & Branson, M. (2020). Interactions between moisture and tropical convection. Part I: The coevolution of moisture and convection. *Journal of the Atmospheric Sciences*, 77(5), 1783–1799. <https://doi.org/10.1175/jas-d-19-0225.1>
- Wolding, B. O., & Maloney, E. D. (2015). Objective diagnostics and the Madden-Julian oscillation. Part II: Application to moist static energy and moisture budgets. *Journal of Climate*, 28(19), 7786–7808. <https://doi.org/10.1175/jcli-d-14-00689.1>
- Wood, R., & Field, P. R. (2011). The distribution of cloud horizontal sizes. *Journal of Climate*, 24(18), 4800–4816. <https://doi.org/10.1175/2011jcli4056.1>
- Yang, B., Wang, M., Zhang, G. J., Guo, Z., Huang, A., Zhang, Y., & Qian, Y. (2021). Linking deep and shallow convective mass fluxes via an assumed entrainment distribution in CAM5-CLUBB: Parameterization and simulated precipitation variability. *Journal of Advances in Modeling Earth Systems*, 13(5), e2020MS002357. <https://doi.org/10.1029/2020ms002357>
- Yang, S., Zhang, T., Li, Z., & Dong, S. (2019). Climate variability over the Maritime Continent and its role in global climate variation: A review. *Journal of Meteorological Research*, 33(6), 993–1015. <https://doi.org/10.1007/s13351-019-9025-x>
- Yoshimura, H., Mizuta, R., & Murakami, H. (2015). A spectral cumulus parameterization scheme interpolating between two convective updrafts with semi-Lagrangian calculation of transport by compensatory subsidence. *Monthly Weather Review*, 143(2), 597–621. <https://doi.org/10.1175/mwr-d-14-00068.1>
- Zhang, C., & Ling, J. (2017). Barrier effect of the Indo-Pacific Maritime Continent on the MJO: Perspectives from tracking MJO precipitation. *Journal of Climate*, 30(9), 3439–3459. <https://doi.org/10.1175/jcli-d-16-0614.1>
- Zhang, G. J., & Song, X. (2009). Interaction of deep and shallow convection is key to Madden-Julian Oscillation simulation. *Geophysical Research Letters*, 36(9), L09708. <https://doi.org/10.1029/2009gl037340>